

Fast-MUSIC for Automotive Massive-MIMO Radar

Bin Li^{1,3}, Shuseng Wang², Jun Zhang³, Xainbin Cao⁴, Chenglin Zhao¹

Abstract—Massive multiple-input multiple-output (MIMO) radar, assisted by millimeter-wave band virtual MIMO techniques, provides great promises to the high-resolution automotive sensing and target detection in unmanned ground/aerial vehicles (UGA/UAV). As one long-standing challenging problem, however existing subspace methods may suffer from either the low resolution/accuracy or the high time complexity. In this study, we propose two computational efficient methods to accomplish the high-resolution estimation of angle of arrival (AoA) information. By leveraging randomized low-rank approximation, our fast-MUSIC approaches, relying on random sampling and projection techniques, would speed up the subspace computation by orders of magnitude. At the same time, we establish the theoretical bounds of our proposed approaches, which ensure the accuracy of approximated pseudo-spectrum. As shown, in the case of high signal-to-noise ratio, the pseudo-spectrum acquired by our fast-MUSIC is highly precise, when compared to the exact MUSIC. Comprehensive numerical study demonstrates that our new methods are tremendously faster than MUSIC, while the AoA estimation accuracy are almost as good as MUSIC. As such, our fast-MUSIC enables the high-resolution yet real-time sensing with massive MIMO radar, which has great potential in the emerging mobile computing and automotive applications.

Index Terms—Millimeter-wave radar, massive MIMO, automotive sensing, fast-MUSIC, mobile computing.

I. INTRODUCTION

Unmanned aircrafts and automotive vehicles are receiving more and more attention from both the industry and academia [1], [2], owing to the great potentials in widespread applications [3]. The success of such unmanned systems critically depends on the fusing of GPS, automotive radar, and other environmental sensors (e.g. lidar, ultrasound, and camera) [4], [5]. In comparison to others sensing techniques, millimeter-wave (mm-wave) automotive radar is extremely attractive to the unmanned systems, due to its two inherent merits. First, it is immune to adverse environment such as dust, fog, and smoke; and second, it is robust to dazzling and no light conditions [6]. Moreover, the recent advancement in mm-wave semiconductor circuit (e.g. 24 and 77GHz) [7]–[10] further makes it possible to deploy large-scale arrays economically to unmanned systems. As such, assisted by virtual Multiple-Input Multiple-Output (MIMO) or co-located MIMO techniques [11], hundreds of reception channels are now made available to achieve the super-resolution environment sensing and target detection in automotive scenarios [12].

In practice, unmanned vehicles typically use three types of mm-wave radars [7]: (1) long-range radar (LRR) for automotive cruise control (i.e. 10-250 m), (2) medium-range radar (LRR) for cross-traffic alert (i.e. 1-100 m), and (3) short-range radar (SRR) for park assist (i.e. 0.15-30 m); see the illustration in Figure 1(a). To meet such diverse requirements, various modulation waveforms have been designed for automotive radars [13], [14]. The popular solutions include frequency-modulated continuous-waveform (FMCW) [15]–[17], pulsed continuous wave (CW) radar, and orthogonal frequency-division multiplexing (OFDM) [18], etc. Among these, FMCW sweeps a wide RF bandwidth (GHz) while keeping simultaneously a small IF bandwidth (MHz), which then permits the high-resolution sensing via low-cost circuit [12], proving great potential for the practical deployment.

Despite great advances in hardware technology and system design of automotive massive-MIMO radar [14], [19], high-resolution yet low-complexity signal processing methods are still lacking. For massive-MIMO radars, the high-resolution environment sensing requires a large number of channels [12], which thus incurs a high computation cost. In automotive scenarios, the computational signal processing may cause an intolerable latency, which potentially leads to the disastrous consequences. So, the deployment of high-resolution massive-MIMO radar in unmanned aircrafts/vehicles calls for an efficient and real-time processing algorithm.

Theoretically, the maximum likelihood (ML) method attains the optimal accuracy [20], which yet requires an exhaustive search in a large two-dimensional space. Provided a large number of signal samples, the subspace methods, represented by Multiple Signal Classification (MUSIC) [21] and Estimation of Signal Parameters via Rational Invariance Techniques (ESPRIT) [22], are expected to attain the near-optimal accuracy [23], which exploits the noise/signal subspace computed by singular value decomposition (SVD) on covariance matrix. Despite great potential to the high-resolution sensing, the high complexity (e.g. $\mathcal{O}(M^3)$ for 1-D estimation, and $\mathcal{O}\{(NM)^3\}$ for 2-D estimation, M is the number of antennas and N is a sample length) and the intolerable latency largely limits their practical use, especially in massive-MIMO radar (e.g. $M > 200$)¹. The dimension of interests in MUSIC can be reduced via pre-estimation [24], which may be still computational (e.g. an extended matrix in 2-D MUSIC is very large).

To simplify subspace algorithms, a block-Lanczos method can be applied [25], which estimates only the first K singular vectors and thereby reduces complexity to $\mathcal{O}(KM^2)$. Besides, a Propagator scheme was designed [26]. By introducing a propagator operator, it simplifies the complexity to $\mathcal{O}(NMK)$

¹ School of Information and Communication Engineering, Beijing University of Posts and Telecommunications, Beijing, 100876, China.

² Department of Computer Science, Stevens Institute of Technology, Hoboken, NJ 07030, USA.

³ School of Information and Electronics, Beijing Institute of Technology, Beijing, 100081, China.

⁴ School of Electronic and Information Engineering, Beihang University, Beijing, 100191, China.

¹For example, when the number of elements is 1000 as in emerging MIMO automotive radars, the processing latency would be around 500 ms even on high-performance CPUs.

(K is the number of targets) [27], which, however, sacrifices the spatial resolution and even the reliability (e.g. in the range of [70, 90] degree) [28]. As a variation of Capon method [29], another matrix-inverse scheme is proposed to avoid SVD and eigenvalue decomposition (EVD) [30], which still has a complexity $\mathcal{O}(M^3)$ and may be unstable when the signal-to-noise-ratio (SNR) is low. As one practical alternative, the target information can be efficiently estimated via FFT [20], [31], [32]. Due to a low complexity, $\mathcal{O}(M \log_2 M)$, it is now adopted by some automotive radars [32], [33], which is yet insufficient to acquire the high-resolution sensing and the high-quality cloud-point information [14].

This work is devoted to break one major bottleneck in automotive massive-MIMO radar. Our goal is to accomplish real-time automotive sensing at a scalable complexity, but achieve the high-resolution target estimation as a near-optimal MUSIC. To accomplish this, we introduce *randomized* low-rank approximation to the angle-of-arrival (AoA) estimations, thus develop two fast-MUSIC methods to approximately compute signal subspace of a large covariance – the general stumbling block in all subspace methods. As such, we are able to achieve the high-resolution AoA estimation at a linear complexity – $\mathcal{O}(K^2 M)$. We expect our fast-MUSIC algorithms would greatly promote the widespread use of automotive massive-MIMO radars to enable unmanned systems.

In summary, our work offers the following contributions.

- We leverage randomized matrix approximation to accelerate the sub-space extraction. To this end, we approximate a large covariance \mathbf{S} via three small matrices, in the form of $\mathbf{S} \simeq \mathbf{C}\mathbf{W}\mathbf{C}^H$. Here, the matrix sketch $\mathbf{C} \in \mathbb{C}^{M \times p}$ ($K < p \ll M$) is abstracted by an uniform column-sampling on \mathbf{S} ; and $\mathbf{W} \in \mathbb{C}^{p \times p}$ is a weighting matrix minimizing the approximation residue. With the randomized low-rank approximation, our fast-MUSIC reduces the complexity of sub-space separation to $\mathcal{O}(p^2 M)$.
- We show our fast-MUSIC approach enables the high-resolution AoA estimation and target detection. As our theoretical analysis suggests, when the signal sub-space is approximately computed as in fast-MUSIC, the acquired pseudo-spectrum $\tilde{P}_{\text{music}}(\theta)$ is at most

$$\mathcal{O}\left(\frac{\sigma_{K+1}(\mathbf{S})}{\sigma_K(\mathbf{S})} \sqrt{\frac{M^2}{p}}\right)$$

times worse than that of the standard MUSIC, when a user-specify parameter meets $p \sim \mathcal{O}(K \log K)$. Here, $\sigma_k(\mathbf{S})$ is the k -th largest singular value of \mathbf{S} . If the signal-to-noise ratio (SNR) is high, then the spectral gap $\frac{\sigma_{K+1}(\mathbf{S})}{\sigma_K(\mathbf{S})}$ is very small, making our estimation accurate.

- To further improve the approximation accuracy, we resort to another random projection method, by iteratively identifying a good orthogonal projection matrix $\mathbf{V} \in \mathbb{C}^{M \times p}$. In contrast to direct random sampling, we thus obtain an improved sketch $\mathbf{C} = \mathbf{S}\mathbf{V} \in \mathbb{C}^{M \times p}$ and the rank-restricted approximation $\mathbf{S} \simeq \mathbf{C}\mathbf{W}\mathbf{C}^H$. By incorporating more information to the sketch \mathbf{C} , the accuracy of the approximated pseudo-spectrum is further promoted.
- We then establish the theoretical bound of our refined algorithm. As analysed, after t iterations, the approximated

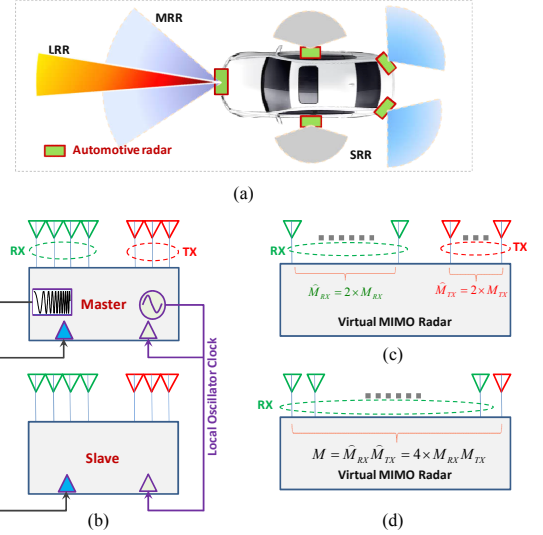


Fig. 1. **Massive MIMO automotive radar with cascaded sub-arrays.** (a) Typical radars for autonomous driving systems, including LRR, MRR and SRR. (b) A schematic framework on cascaded MIMO radar, whereby the master generates the local oscillator signal and controls the slave via two synchronized clocks, i.e. FMCW clock and LO clock. Here, each co-located MIMO radar is equipped with $M_{TX} = 3$ transmitting antennas and $M_{RX} = 4$ receiving antennas. (c) The equivalent MIMO radar system of two cascaded sub-systems. (d) The cascaded-based massive MIMO radar system with the equivalent channels of $M = 4 \times M_{RX} M_{TX}$.

pseudo-spectrum $\tilde{P}_{\text{music}}(\theta)$ is at most

$$\mathcal{O}\left(\left(\frac{\sigma_{K+1}(\mathbf{S})}{\sigma_K(\mathbf{S})}\right)^{t+1} \sqrt{M^2 K}\right)$$

times worse than that of the standard MUSIC. If the SNR is high, several power iterations (e.g. $t = 2$) would suffice for the near-optimal estimation.

- We conduct comprehensive simulations to evaluate our fast-MUSIC methods and compare them with its counterparts such as MUSIC, Lanczos, Propagator, etc. Our numerical studies demonstrate the efficiency and accuracy of fast-MUSIC, which provides the great potential to high-resolution and real-time massive-MIMO radars in the emerging mobile and automotive applications.

The remaining of this work is structured as follows. In Section II, we briefly introduce the system model and current subspace algorithms for automotive sensing. In Section III, we present two fast-MUSIC methods inspired by randomised matrix approximation. In Section IV, we derive some theoretical bounds of interests. In Section V, the numerical simulations are provided. Finally, we conclude this work in Section VI.

The used notations are summarized as follows: \mathbf{A} denotes a matrix with a rank $r = \text{rank}(\mathbf{A})$; its SVD is $\mathbf{A} = \mathbf{U}\mathbf{\Sigma}\mathbf{V}^H = \sum_{i=1}^r \sigma_i(\mathbf{A}) \mathbf{u}_i \mathbf{v}_i^H$, where $\sigma_i(\mathbf{A}) (> 0)$ is the i -th singular value; \mathbf{u}_i and \mathbf{v}_i are the i -th left and right singular vector. The Moore-Penrose pseudo-inverse of \mathbf{A} is \mathbf{A}^\dagger . The spectral norm of \mathbf{A} is $\|\mathbf{A}\|_2 = \sigma_1(\mathbf{A})$. The F-norm of \mathbf{A} is $\|\mathbf{A}\|_F = \sqrt{\text{tr}(\mathbf{A}^H \mathbf{A})}$. The best rank- k ($k < r$) approximation to \mathbf{A} is $\mathbf{A}_k \triangleq \sum_{i=1}^k \sigma_i(\mathbf{A}) \mathbf{u}_i \mathbf{v}_i^H$. For the $M \times K$ matrix with orthonormal columns \mathbf{U}_K , its row coherence of \mathbf{U}_K is defined as $\mu(\mathbf{U}_K) \triangleq \frac{M}{K} \max_i \|(\mathbf{U}_K)_i\|_2^2 \in [1, \frac{M}{K}]$, where $(\mathbf{U}_K)_i$ is the i -th row of \mathbf{U}_K .

II. SYSTEM MODEL

In this section, we briefly introduce a FMCW radar system for autonomous systems, as well as the popular subspace algorithms for parameter estimation and target detection.

A. FMCW Radar System

Assume the massive-MIMO radar system (e.g. virtual MIMO) consisting of M antennas, i.e. the uniform linear array (ULA). For each antenna element, the emitted FMCW waveform within a symbol duration T_{sym} reads [15], [32]:

$$s(t) = \exp \left[j \left(w_s t + \frac{\mu}{2} t^2 \right) \right], \quad 0 \leq t < T_{\text{sym}}, \quad (1)$$

where w_s is the initial frequency and μ is the changing rate of instantaneous frequency of the chirp signals. Given the bandwidth of FMCW signals, w_B , as well as an emission duration, T_{sym} , the changing rate is then $\mu = w_B / T_{\text{sym}}$.

Suppose there are K target points to be estimated. We thus need to estimate their ToAs and AoAs, denoted respectively as τ_k and θ_k , for $k = 0$ to $K - 1$. After the signal calibration, the received signal at the m -th antenna reads:

$$y_m(t) = \sum_{k=0}^{K-1} \alpha_{k,m} s(t - \tau_k) \times \exp \left(j \frac{2\pi}{\lambda_s} m d \sin \theta_k \right) + n_m(t).$$

Here, $r_k(t) \triangleq \alpha_{k,m} s(t - \tau_k)$ is the signal reflected from the k -th target; $\alpha_{k,m}$ is the complex channel gain between the k -th target and the m -th element, and in far-field cases we have $\alpha_{k,m} = \alpha_k$; λ_s denotes the wavelength of signal carrier; d is the spacing distance of two adjacent elements (we assume $d = \lambda_s / 2$); $n_m(t) \sim \mathcal{N}(0, \sigma_n^2)$ is additive Gaussian noise.

An advantage of FMCW radar is that it is able to demodulate signals via the simple mixer [15], which greatly facilitates the low-cost radio-frequency (RF) implementation [33]. To be specific, at reception-end the mixer-based de-chirping process is firstly applied to attain the beat signal $\tilde{y}_m(t)$, i.e.

$$\tilde{y}_m(t) = s(t) \times \left[\sum_{k=0}^{K-1} r_k(t) \exp \left(j \frac{2\pi}{\lambda_s} m d \sin \theta_k \right) + n_m(t) \right].$$

With $s(t)$ substituting by eq. (1), and after a low-pass filter with an impulse response $h(t)$, the beat signal is obtained, which is a composition of target-modulated sinusoidal signals:

$$\tilde{y}_m(t) = \sum_{k=0}^{K-1} \alpha_k e^{j(\mu \tau_k t + \omega_s \tau_k - \frac{\mu}{2} \tau_k^2)} \cdot e^{j(\pi k \sin \theta_k)} + \tilde{n}_m(t).$$

Here, $\tilde{n}_m(t) = h(t) \otimes [n_m(t)s(t)]$ is the residual noise after the de-chirping processing, while \otimes denotes the convolution process. Then, an analog to digital convertor (ADC) with sampling frequency $f_s = 1/T_s$ outputs the discrete signal:

$$\tilde{y}_m(n) = \tilde{y}_m(nT_s),$$

for $m = 0$ to $M - 1$ and $n = 0$ to $N - 1$, with $N = T_{\text{sym}}/T_s$. On this basis, the discrete beat signal $y_m(n)$ would contain the angle-induced phase shift ϑ_k , delay-induced phase shift κ_k ,

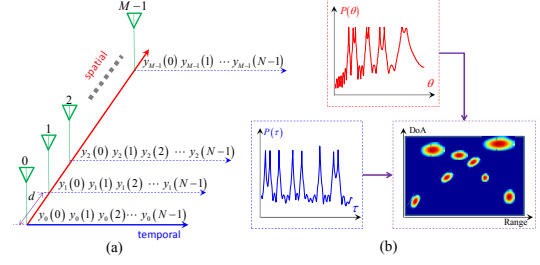


Fig. 2. Schematic paradigm of unknown targets detection and estimation. (a) Taking ULA for example, the data-flow of multiple channels (i.e. M) are structured into a data matrix, $\mathbf{Y} \in \mathbb{C}^{M \times N}$. (b) The AoAs and time delays of K sources are computed using $\mathbf{S} = \frac{1}{N} \mathbf{Y} \mathbf{Y}^H$ and $\mathbf{T} = \frac{1}{M} \mathbf{Y}^H \mathbf{Y}$. Further with either a 2-D or the low-complexity 1-D pairing mechanisms [30], [34], the range-angle (R-A) plane is attained.

and delay-induced phase ρ_k , with which the unknown AoA, ToA and range information can be recovered.

$$\vartheta_k = \exp \left[j \frac{2\pi}{\lambda_s} d \sin(\theta_k) \right], \quad (2)$$

$$\kappa_k = \exp(j \mu \tau_k T_{\text{sym}}), \quad (3)$$

$$\rho_k = \exp \left[j \left(-\frac{1}{2} \mu \tau_k^2 + w_s \tau_k \right) \right]. \quad (4)$$

In the following, we examine the subspace-based high-resolution AoAs estimation of targets. Such an information is of great importance to unmanned systems, which yet poses a major challenge to real-time automotive sensing.

B. Subspace-based Targets Detection & Estimation

In the automotive environment sensing, unknown AoA, θ_k , and the temporal delay, τ_k , can be estimated via many different methods. When the high resolution estimation is particularly emphasised, the subspace methods tend to be preferable. Popular subspace methods, such as MUSIC [21], [35] and ESPRIT [22], all start from the temporal covariance matrix or the spatial covariance matrix (Figure 2), i.e.

$$\mathbf{S} = \frac{1}{N} \mathbf{Y} \mathbf{Y}^H, \quad \mathbf{T} = \frac{1}{M} \mathbf{Y}^H \mathbf{Y}, \quad (5)$$

whereby the signal matrix $\mathbf{Y} \in \mathbb{C}^{M \times N}$ is arranged as:

$$\mathbf{Y} \triangleq \begin{bmatrix} \tilde{y}_0(0) & \tilde{y}_0(1) & \cdots & \tilde{y}_0(N-1) \\ \tilde{y}_1(0) & \tilde{y}_1(1) & \cdots & \tilde{y}_1(N-1) \\ \vdots & \vdots & \ddots & \vdots \\ \tilde{y}_{M-1}(0) & \tilde{y}_{M-1}(1) & \cdots & \tilde{y}_{M-1}(N-1) \end{bmatrix}. \quad (6)$$

There are two important things to be noted for the above covariance matrix. First, the matrix multiplication in computing \mathbf{S} incurs also high complexity, which yet can be efficiently implemented in parallel. Second, for massive-MIMO radars (with the large M), the required sample length N will be infinite, in order to estimate an unbiased covariance via eq. (5). For a finite length, the standard estimate of MUSIC pseudo-spectrum may be inconsistent [36], e.g. due to the inaccurate estimate of \mathbf{S} [37]. Such theoretical limitations of standard MUSIC, however, may be overcome by the post-processing algorithm, e.g. refining the estimated pseudo-spectrum via well-designed weights [38], [39]. Recently, the single-snapshot

MUSIC scheme was studied [40]. As demonstrated, even in the special case $N = 1$, the super-resolution AoA estimation can be attained via a time-delayed Hankle matrix [40].

Note that, the emphasis of this work yet puts on the subspace approximation in acquiring the AoA / ToA estimations. Without losing generality, here we take the example of estimating AoAs, provided the covariance matrix \mathbf{S} ; whilst the estimation of ToAs may be similarly accomplished with \mathbf{T} . Assume there are K unknown target points, we first compute the SVD of a large covariance $\mathbf{S} \in \mathbb{C}^{M \times M}$, i.e.

$$\mathbf{S} = \mathbf{U}\mathbf{\Sigma}\mathbf{V}^H = \mathbf{U}_K\mathbf{\Sigma}_K\mathbf{V}_K^H + \epsilon_n^2\mathbf{U}_{-K}\mathbf{V}_{-K}^H, \quad (7)$$

where $\mathbf{U}_K = [\mathbf{u}_1, \dots, \mathbf{u}_K] \in \mathbb{C}^{M \times K}$ corresponds to signal subspace, and $\mathbf{U}_{-K} = [\mathbf{u}_{K+1}, \dots, \mathbf{u}_M] \in \mathbb{C}^{M \times (M-K)}$ corresponds to noise subspace. For a Hermitian matrix $\mathbf{S}^H = \mathbf{S}$, we further have $\mathbf{V} = \mathbf{U}$. As common, we assume $\sigma_1(\mathbf{S}) > \sigma_2(\mathbf{S}) > \dots > \sigma_M(\mathbf{S})$, and $\sigma_m(\mathbf{S}) = \epsilon_n^2$ ($m > K$).

Then, we uniformly partition the spatial angle range $[0, \pi]$ into a grid of L values, $\{\theta_0, \theta_1, \dots, \theta_{L-1}\}$. For each angle θ_l , we define the M -dimensional steering vector:

$$\mathbf{a}(\theta) \triangleq [a_0(\theta), a_1(\theta), \dots, a_{M-1}(\theta)]^H$$

where

$$a_m(\theta) = \exp\left(\frac{j 2\pi d m \sin(\theta)}{\lambda}\right), \quad \text{for } m = 0, 1, \dots, M-1.$$

Finally, we are able to evaluate the standard MUSIC pseudo-spectrum, by fully utilizing the subspace information:

$$P_{\text{music}}(\theta) = \frac{1}{\mathbf{a}(\theta)^H \mathbf{U}_{-K} \mathbf{U}_{-K}^H \mathbf{a}(\theta)} = \frac{1}{\mathbf{a}(\theta)^H (\mathbf{I}_M - \mathbf{U}_K \mathbf{U}_K^H) \mathbf{a}(\theta)}. \quad (8)$$

In practice, $P_{\text{music}}(\theta)$ needs to be estimated for every $\theta \in \{\theta_0, \dots, \theta_{L-1}\}$. Given a signal subspace \mathbf{U}_K , the evaluation of the whole pseudo-spectrum $P_{\text{music}}(\theta)$ requires a complexity $\mathcal{O}(MKL)$. Fortunately, the evaluation of $P_{\text{music}}(\theta)$ can be performed in parallel, indicating the actual time cost would be much lower than $\mathcal{O}(MKL)$. Besides, once provided \mathbf{U}_K , the more effective evaluation of $P_{\text{music}}(\theta)$ can be realized by another ESPRIT method [22] or root-MUSIC scheme, which, however, is out of scope of this current work. Thus, we will focus on the efficient computation of signal subspace \mathbf{U}_K , by presenting new approaches to reduce the complexity.

As shown by Figure 2(b), each peaks of the MUSIC pseudo-spectrum $P_{\text{music}}(\theta)$ indicate one target point. Following this, unknown target AoAs, θ_k ($k = 0, 1, \dots, K-1$), are then extracted by identifying multiple peaks in $P_{\text{music}}(\theta)$, i.e.

$$\hat{\theta} = \{\theta_k, \theta_k = \text{peak}\{P_{\text{music}}(\theta)\}\}. \quad (9)$$

In the above, we elaborate a standard MUSIC method, which would compute AoAs and ToAs successively [30], [34], i.e. via a 1-D pseudo-spectrum. Besides, there is also another 2-D MUSIC algorithm, which is able to estimate K ToAs and AoAs jointly at once [41], [42], e.g. via the SVD on an extended $MN \times MN$ covariance matrix.

In the following, we are devoted to reduce the time complexity of the 1-D MUSIC method. As discussed above, its complexity comes mainly from the matrix decomposition of a large covariance \mathbf{S} , which is measured by $\mathcal{O}(M^3)$; and meanwhile, there is no parallel algorithm to accelerate it. Despite

TABLE I
TIME COMPLEXITIES OF CLASSICAL DOA ESTIMATION METHODS

Methods	Complexity	Resolution	Conditions
MUSIC	$\mathcal{O}(M^3)$	high	all
Lanczos	$\mathcal{O}(KM^2)$	high	all
Matrix-inverse	$\mathcal{O}(M^3)$	high	$\epsilon_n \rightarrow 0$
Propagator	$\mathcal{O}(KMN)$	medium	$ \theta \leq 70^\circ$
FFT Method	$\mathcal{O}(M \log M)$	low	all
Fast MUSIC 1	$\mathcal{O}(Mp^2)$	high	$K \ll M$
Fast MUSIC 2	$\mathcal{O}(tpM^2)$	high	$K \ll M$

1. Here, p ($K \leq p \ll M$) is an over-sampling parameter; t ($t \geq 1$) is the number of iterations in updating the projection matrix.

2. Note that, the real complexity of our fast method 2 is largely lower than $\mathcal{O}(tpM^2)$, as the polynomial complexity on M comes from the matrix multiplication which is yet more efficient than SVD or matrix inverse.

the high-resolution automotive sensing with massive-MIMO radars, the computation latency would be too long (> 100 ms for $M > 500$), by potentially causing disastrous results.

C. Simplification of Subspace-based Estimation

There are many works target at reducing the computational complexity of subspace methods, which may have different advantages and disadvantages, as summarized in Table I.

1) **Lanczos Method:** A direct solution is to integrate the Lanczos algorithm into MUSIC. Taking the block-Lanczos scheme for example, one may tend to estimate only the first K singular vectors and thus form a signal subspace \mathbf{U}_K , rather than computing the whole singular matrix \mathbf{U} . A block-Lanczos method thus requires a complexity $\mathcal{O}(KM^2)$. Although it may obtain the exact pseudo-spectrum as in MUSIC, its time latency was still intolerable for real-time automotive sensing with massive-MIMO radars (e.g. $M > 200$).

2) **Matrix-inverse Method:** The recent work [30] suggests to replace the computational SVD via the matrix inverse which may have more efficient algorithms. From eq. (7), we have:

$$\mathbf{S}^{-1} = \mathbf{U}_K \mathbf{\Sigma}_K^{-1} \mathbf{U}_K^H + \frac{1}{\epsilon_n^2} \mathbf{U}_{-K} \mathbf{U}_{-K}^H \approx \frac{1}{\epsilon_n^2} \mathbf{U}_{-K} \mathbf{U}_{-K}^H. \quad (10)$$

Even through this may reduce time cost to some extents, a matrix inverse still has a complexity $\mathcal{O}(M^3)$. Moreover, this method requires high SNR to make the approximation in (10) accurate (e.g. the above approximation holds only when ϵ_n is very small). In low SNRs, the approximated noise subspace should be less accurate, making $P_{\text{inv}}(\theta)$ largely deviated from the standard MUSIC pseudo-spectrum.

3) **Propagator Method:** Different from the extract subspace identified by SVD, the Propagator method resorts to a special partition of signal matrix $\mathbf{Y} = [\mathbf{Y}_1 \in \mathbb{C}^{K \times N}; \mathbf{Y}_2 \in \mathbb{C}^{(M-K) \times N}]$. It seeks for a transform matrix among two above partitions, i.e. $\mathbf{Y}_2 = \mathbf{P}_{\text{pro}}^H \mathbf{Y}_1$. After determining this transform matrix \mathbf{P}_{pro} , both signal and noise subspace are respectively constructed [26]. Finally, a spatial pseudo-spectrum is approximated via the new approximated signal/noise subspace. In this respect, the Propagator method has a very low complexity $\mathcal{O}(MNK)$. Unfortunately, it provides low-resolution and uncertain results in specific spatial ranges.

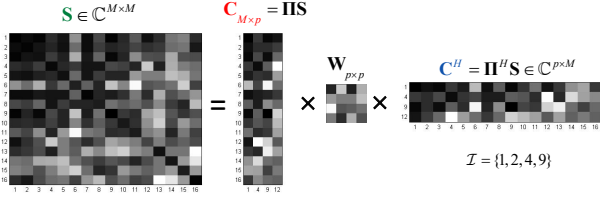


Fig. 3. Illustration of randomized low-rank approximation of a large covariance matrix $\mathbf{S} \in \mathbb{R}^{N \times N}$. Here, the randomly selected column indexes set is $\mathcal{I} = \{1, 4, 2, 9\}$. Thus, the low-dimensional sketch \mathbf{C} consists of $p = |\mathcal{I}| = 4$ columns of \mathbf{S} , while \mathbf{C}^H involves 4 rows.

From the above comparison, one long-standing challenge in MIMO radar signal processing is that the high resolution and the low complexity constitute an inherent contradiction. As noted in Table I, current subspace methods mainly aims to a compromise between two contradictory objectives.

III. LOW-RANK APPROXIMATIONS

In contrast to the exact matrix computation / decomposition, e.g. SVD and K -SVD, we leverage randomized low-rank approximation to perform automotive sensing with massive-MIMO radars, which allows for both high-resolution AoAs estimation and the linearly scalable complexity. To this end, we develop two fast-MUSIC algorithms to compute the approximated pseudo-spectrum, inspired by random sampling and random projection techniques, respectively. Note that, such randomized matrix sketching methods have been studied in linear algebra and scientific computing [43]–[45]. To the best of our knowledge, however, this would be the first attempt to use them to solve the long-standing challenging problem in massive-MIMO radars.

A. Fast MUSIC Method – 1

In fast-MUSIC, we are concerned with the efficient estimation of a signal subspace and the high-resolution DoA at a scalable linear complexity. To accomplish this, we may approximate the large covariance matrix $\mathbf{S} \in \mathbb{C}^{M \times M}$ by 3 small matrices, which are known also as sketches, in a special form $\mathbf{S} \simeq \mathbf{C} \mathbf{W} \mathbf{C}^H$, as illustrated in Figure 3. Meanwhile, in order to reduce the time complexity to the maximum, we resort to a simple random sampling technique to abstract the involved matrix sketch $\mathbf{C} \in \mathbb{C}^{M \times p}$ ($K \leq p \ll M$) from \mathbf{S} .

To be specific, we first configure an over-sampling parameter p , and then uniformly sample p items from $\{0, 1, \dots, M-1\}$ to form the indexing set \mathcal{I} , i.e. $|\mathcal{I}| = p$. Then, a sketching matrix is structured as $\mathbf{C} = \mathbf{S}(:, \mathcal{I}) = \mathbf{S} \mathbf{\Pi}$, where $\mathbf{\Pi} \in \mathbb{R}^{M \times p}$ is the equivalent sampling matrix. So, $\mathbf{C} \in \mathbb{R}^{M \times p}$ contains the p columns of \mathbf{S} indexed by \mathcal{I} . In this sampling matrix $\mathbf{\Pi}$, there are p columns contains only one non-zero entry $\sqrt{M/p}$ (the remaining $M - p$ columns are all zeros).

By minimizing the matrix approximation error, we further obtain another weight matrix \mathbf{W}_{opt} , i.e.

$$\mathbf{W}_{opt} = \arg \min_{\mathbf{W}} \|\mathbf{S} - \mathbf{C} \mathbf{W} \mathbf{C}^H\|_F^2 = \mathbf{C}^\dagger \mathbf{S} \mathbf{C}^{\dagger H}. \quad (11)$$

Since the involved pseudo-inverse and matrix multiplication have the high complexity, we tend to the other efficient

Algorithm 1 Fast MUSIC Method – 1.

- 1: **Input:** a covariance matrix \mathbf{S} , the number of target points K , and over-sampling parameter p ($\geq K$).
- 2: // **Step 1:** Random Sampling Method
- 3: $\mathcal{I} \leftarrow$ randomly sampling p indices from $\{0, 1, \dots, M\}$;
- 4: $\mathbf{C} \leftarrow$ the column of \mathbf{S} indexed by \mathcal{I} ;
- 5: $\mathbf{W} \leftarrow$ the pseudo-inverse of $\mathbf{S}(\mathcal{I}, \mathcal{I})$;
- 6: // **Step 2:** Rank Restriction
- 7: Compute the SVD of $\mathbf{C} = \mathbf{U}_c \mathbf{\Sigma}_c \mathbf{V}_c^H$;
- 8: Compute the SVD: $\mathbf{\Sigma}_c \mathbf{V}_c^H \mathbf{W} \mathbf{V}_c \mathbf{\Sigma}_c^T = \mathbf{U}_B \mathbf{\Sigma}_B \mathbf{V}_B^H$;
- 9: Compute the signal subspace: $\tilde{\mathbf{U}}_K \leftarrow \mathbf{U}_c \mathbf{U}_B$;
- 10: // **Step 3:** Approximate MUSIC
- 11: Compute $\tilde{P}_{music}(\theta) = \frac{1}{\mathbf{a}(\theta)^H \mathbf{a}(\theta) - \mathbf{a}(\theta)^H \tilde{\mathbf{U}}_K \tilde{\mathbf{U}}_K^H \mathbf{a}(\theta)}$ for all θ .

methodology to compute \mathbf{W} . I.e., we may solve the above over-determined system in eq. (11), by sketching both \mathbf{S} and its random approximation. This leads to the so-called Nyström approximation [43], [46], with a weight matrix

$$\mathbf{W} = \arg \min_{\mathbf{W}} \|\mathbf{\Pi}^H (\mathbf{S} - \mathbf{C} \mathbf{W} \mathbf{C}^H) \mathbf{\Pi}\|_F^2 = (\mathbf{\Pi}^H \mathbf{S} \mathbf{\Pi})^\dagger. \quad (12)$$

Finally, a large covariance matrix \mathbf{S} is approximated by:

$$\mathbf{S} \simeq \tilde{\mathbf{S}} \triangleq \mathbf{C} \mathbf{W} \mathbf{C}^H. \quad (13)$$

Relying on the above approximate representation of \mathbf{S} , its SVD can be efficiently computed via multiple SVDs of small matrices. To be specific, given $\mathbf{C} = \mathbf{U}_c \mathbf{\Sigma}_c \mathbf{V}_c^H$, the covariance matrix \mathbf{S} would be further approximated by:

$$\mathbf{S} \simeq \mathbf{U}_c \mathbf{\Sigma}_c \mathbf{V}_c^H \mathbf{W} (\mathbf{U}_c \mathbf{\Sigma}_c \mathbf{V}_c^H)^H.$$

After defining $\mathbf{B} \triangleq \mathbf{\Sigma}_c \mathbf{V}_c^H \mathbf{W} \mathbf{V}_c \mathbf{\Sigma}_c^H$ and computing its SVD, i.e. $\mathbf{B} = \mathbf{U}_B \mathbf{\Sigma}_B \mathbf{V}_B^H$, we obtain the rank-restricted approximate SVD of \mathbf{S} , i.e.

$$\mathbf{S} \simeq \mathbf{U}_c \mathbf{U}_B \mathbf{\Sigma}_B \mathbf{V}_B^T \mathbf{U}_c^H = \tilde{\mathbf{U}}_K \mathbf{\Sigma}_B \tilde{\mathbf{U}}_K^H,$$

whereby $\tilde{\mathbf{U}}_K \triangleq \mathbf{U}_c \mathbf{U}_B$ forms a unitary matrix. Up to now, we obtain the approximated signal subspace $\tilde{\mathbf{U}}_K$, and relying on it we estimated the approximated pseudo-spectrum by

$$\tilde{P}_{music}(\theta) = \frac{1}{\mathbf{a}(\theta)^H (\mathbf{I}_M - \tilde{\mathbf{U}}_K \tilde{\mathbf{U}}_K^H) \mathbf{a}(\theta)}. \quad (14)$$

A schematic flow of our fast-MUSIC method 1 is summarized in Algorithm 1, which actually approximates the rank-restricted SVD of large covariance, and significantly reduced the complexity. Based on the above elaboration, we easily find that: Step 1 (Lines 2 to 5) costs $\mathcal{O}(pM)$ time. Step 2 (Lines 6 to 9) costs $\mathcal{O}(p^2M)$ time. Thus, the overall complexity of our fast method 1 in identifying a signal subspace is $\mathcal{O}(p^2M)$.

B. Fast MUSIC Method – 2

The above random sampling technique enables a highly efficient approximation of the large covariance and the MUSIC pseudo-spectrum. In fact, the above approximated pseudo-spectrum in eq. (14) is accurate, which suffices to attain the high-resolution DoAs estimation. However, one potential problem is that, in the worst-case, its error bound is relatively weak; see Section IV-C for the theoretical analysis.

If the precise matrix approximation is emphasized, we may resort to the other random projection technique [47]. Here, a major difference with regards to our fast method 1 is that, when abstracting the small sketch \mathbf{C} , a more informative projection matrix $\mathbf{\Pi} \in \mathbb{C}^{M \times p}$ is used, i.e. $\mathbf{C} = \mathbf{S}\mathbf{\Pi}$, which is computed via an iterative process. Compared with the random sampling based sketch in Algorithm 1, such a random projection based sketch should incorporate more information of \mathbf{S} and thus permits a more accurate approximation.

To begin with, we first initialize one $M \times p$ random matrix $\mathbf{\Pi}$, whose entries are all i.i.d. values from a Normal distribution $\mathcal{N}(0, 1)$. Then, we obtain a randomly projected sketch $\mathbf{C}^{(1)} = \mathbf{S}\mathbf{\Pi} \in \mathbb{C}^{M \times p}$. To improve the sketching quality, we further compute the orthonormal basis of this projected sketch $\mathbf{C}^{(1)}$, i.e.

$$[\mathbf{Q}_c, \mathbf{R}_c] = \text{qr}(\mathbf{S}\mathbf{\Pi}), \quad \mathbf{V}^{(1)} \triangleq \mathbf{Q}_c,$$

where $\text{qr}(\cdot)$ denotes the QR decomposition, and therefore the $M \times p$ matrix \mathbf{V} gives an improved projection matrix. Subsequently, we obtain another updated sketch $\mathbf{C}^{(2)} = \mathbf{S}\mathbf{V}^{(1)} \in \mathbb{C}^{M \times p}$, and further obtain its orthonormal basis $\mathbf{V}^{(2)}$, i.e.

$$[\mathbf{Q}_c, \mathbf{R}_c] = \text{qr}(\mathbf{S}\mathbf{V}^{(1)}), \quad \mathbf{V}^{(2)} \triangleq \mathbf{Q}_c. \quad (15)$$

The above process is repeated for t times, and thus we achieve a good matrix sketch $\mathbf{C}^{(t)} = \mathbf{S}\mathbf{V}^{(t)} \in \mathbb{C}^{M \times p}$. Similar to eq. (12), the $p \times p$ weight matrix is the computed via:

$$\mathbf{W} = \left(\mathbf{V}^{(t)H} \mathbf{S} \mathbf{V}^{(t)} \right)^\dagger.$$

With $\mathbf{C} = \mathbf{C}^{(t)}$ and \mathbf{W} at hand, we are able to attain the projection-based matrix approximation, $\mathbf{S} \simeq \mathbf{C}\mathbf{W}\mathbf{C}^H$. In the same way, the SVD of \mathbf{S} is approximately attained by multiple SVDs on small matrices, $\mathbf{S} \simeq \tilde{\mathbf{U}}_K \mathbf{\Sigma}_B \tilde{\mathbf{U}}_K^H$. Finally, the pseudo-spectrum $\tilde{P}_{\text{music}}(\theta)$ is approximately estimated via eq. (14).

The time complexity of our fast method 2 is measured by $\mathcal{O}(tpM^2)$. Note that, despite a similar random projection as for Lanczos, our method targets at deriving small sketches and a matrix approximation in eq. (13), which is hence much faster than the SVD of \mathbf{S} and the other block-Lanczos method². As shown by our theoretical analysis in Section IV-C, the user-specific parameter t trades off the complexity and the accuracy. A large t improves the projection matrix and the matrix approximation accuracy, but also increases the complexity.

IV. PERFORMANCE BOUNDS FOR FAST-MUSIC

In practice, our primary concern is the accuracy of $\tilde{P}_{\text{music}}(\theta)$ relative to its exact version $P_{\text{music}}(\theta)$. In this section, we thus analyze the theoretical performance of our fast-MUSIC approaches, i.e. the relative error between our approximate pseudo-spectrum in eq. (14) and the exact pseudo-spectrum in eq. (8) which utilizes the exact signal subspace \mathbf{U}_K .

²Here, although the theoretical complexity is relatively high, the actual time cost of our fast method 2 is very low. Note that, the iterative random projection involves two parts: (1) matrix multiplication requiring a complexity $\mathcal{O}(pM^2)$, (2) the QR decomposition having a complexity $\mathcal{O}(p^2M)$. As the matrix multiplication is highly efficient, the whole complexity is dramatically lower than the Lanczos method, as validated by the following numerical result.

Algorithm 2 Fast MUSIC Method 2.

- 1: **Input:** spatial covariance matrix \mathbf{S} ($M \times M$) and target rank K .
 - 2: // **Step 1: Random Projection**
 - 3: $\mathbf{\Pi} \leftarrow M \times K$ matrix with entries i.i.d. drawn from $\mathcal{N}(0, 1)$;
 - 4: Random projection based matrix sketch: $\mathbf{C} \leftarrow \mathbf{S}\mathbf{\Pi}$;
 - 5: Repeat $\mathbf{V} \leftarrow \text{orth}(\mathbf{C})$ and $\mathbf{C} \leftarrow \mathbf{S}\mathbf{V}$ for t times;
 - 6: // **Step 2: Randomized Matrix Approximation**
 - 7: $\mathbf{C} \leftarrow \mathbf{S}\mathbf{V}$ and $\mathbf{W} \leftarrow (\mathbf{V}^H \mathbf{S} \mathbf{V})^\dagger$;
 - 8: Compute the SVD of $\mathbf{C} = \mathbf{U}_c \mathbf{\Sigma}_c \mathbf{V}_c^H$;
 - 9: Compute the SVD: $\mathbf{\Sigma}_c \mathbf{V}_c^H \mathbf{W} \mathbf{V}_c \mathbf{\Sigma}_c^T = \mathbf{U}_B \mathbf{\Sigma}_B \mathbf{V}_B^H$;
 - 10: Compute the signal subspace: $\tilde{\mathbf{U}}_K \leftarrow \mathbf{U}_c \mathbf{U}_B$;
 - 11: // **Step 3: Approximate MUSIC**
 - 12: Compute $\tilde{P}_{\text{music}}(\theta) = \frac{1}{\mathbf{a}(\theta)^H \mathbf{a}(\theta) - \mathbf{a}(\theta)^H \tilde{\mathbf{U}}_K \tilde{\mathbf{U}}_K^H \mathbf{a}(\theta)}$ for all θ .
-

It should be noted that, from the theoretical perspective, existing theories or error bounds developed for randomized matrix sketching would become inapplicable to our problem. In this study, the ultimate aim of our fast-MUSIC is to approximate an exact pseudo-spectrum $P_{\text{music}}(\theta)$ and acquire the high-resolution AoAs estimation. Unfortunately, most existing theories [43], [44], [47] bound only the matrix norm errors, e.g. $\|\mathbf{S} - \tilde{\mathbf{S}}\|_F$ or $\|\mathbf{S} - \tilde{\mathbf{S}}\|_2$. Thus, such matrix norm bounds should not lend any support to our fast-MUSIC methods.

In the following, we show the relative error of our estimated $\tilde{P}_{\text{music}}(\theta)$ is also bounded, after approximating \mathbf{S} with $\tilde{\mathbf{S}}$, which is more difficult than deriving traditional matrix norm bounds. Our Theorems 1 and 2 establish lower bounds for $\tilde{P}_{\text{music}}(\theta)$. Theorem 3 establishes an upper bound for it.

A. Lower/Upper Bounds of $\tilde{P}_{\text{music}}(\theta)$

First, we expect to have an *lower bound* in the following form: there is a bounded positive number α_l such that

$$\tilde{P}_{\text{music}}(\theta) \geq \frac{1}{1+\alpha_l} P_{\text{music}}(\theta) \quad (16)$$

for all θ . Such a lower bound is of great significance, as it guarantees that our approximated pseudo-spectrum $\tilde{P}_{\text{music}}(\theta)$ will not make the target peaks disappear (see the theoretical analysis in Section IV-E). Theorems 1 and 2 are such lower bounds for our fast methods 1 and 2, respectively.

Second, we expect to have an *upper bound* in the following form: there is a bounded positive number α_u such that

$$\tilde{P}_{\text{music}}(\theta) \leq \frac{1}{1-\alpha_u} P_{\text{music}}(\theta) \quad (17)$$

for all θ . Such an upper bound guarantees that our approximated pseudo-spectrum $\tilde{P}_{\text{music}}(\theta)$ will not interpret a non-peak as a false target peak (see the analysis Section IV-E). Theorem 3 is such an upper bound for the fast method 2. As for the fast method 1, we do not have such an upper bound at the current stage, which will be left to the future work.

B. Lower Bounds for Fast Method 1

Let $\mathbf{S}_K = \mathbf{U}_K \mathbf{\Sigma}_K \mathbf{U}_K^H$ be the best rank- K approximation to \mathbf{S} , and $\tilde{\mathbf{S}} = \mathbf{C}\mathbf{W}\mathbf{C}^H$ be randomized matrix approximation to \mathbf{S} via uniform column sampling (i.e. $\mathbf{C} = \mathbf{S}\mathbf{\Pi}$ and $\mathbf{\Pi}$ is the sampling matrix); and $\tilde{\mathbf{U}}$ be the orthonormal basis of $\tilde{\mathbf{S}}$.

Theorem 1. Let the notation be defined in the above. Let $\delta \in (0, 1)$ be any user-specified constant and $\mu(\mathbf{U}_K)$ be the coherence of \mathbf{U}_K . For a user-specific sampling parameter

$$p \geq 4.5 \mu(\mathbf{U}_K) K \cdot \log \frac{K}{\delta},$$

the following relation holds with probability at least $1 - \delta$:

$$\sqrt{\frac{P_{\text{music}}(\theta)}{\tilde{P}_{\text{music}}(\theta)}} \leq 1 + 2\sqrt{\frac{M^2}{p} \frac{\sigma_{K+1}(\mathbf{S})}{\sigma_K(\mathbf{S})}}. \quad (18)$$

Here, Theorem 1 establishes a lower bound on $\tilde{P}_{\text{music}}(\theta)$, as in eq. (18). The relative approximation error is basically

$$\mathcal{O}\left(2\sqrt{\frac{M^2}{p} \cdot \frac{\sigma_{K+1}(\mathbf{S})}{\sigma_K(\mathbf{S})}}\right).$$

If the SNR is high, then we have $\sigma_K(\mathbf{S}) \gg \sigma_{K+1}(\mathbf{S}) = \epsilon_n^2$; and therefore; the approximation error would be very small.

C. Lower Bound for Fast Method 2

Let $\mathbf{\Pi}$ be an $M \times p$ initial projection matrix with i.i.d. entries drawn from $\mathcal{N}(0, 1)$. Let the $M \times p$ matrix $\mathbf{V}^{(t)}$ be an improved projection matrix after t iterations; in other words, $\mathbf{V}^{(t)}$ is the orthonormal basis of $\mathbf{S}^t \mathbf{\Pi}$. By definition, $\mathbf{C} = \mathbf{S} \mathbf{V}^{(t)}$ and $\mathbf{W} = (\mathbf{V}^{(t)H} \mathbf{S} \mathbf{V}^{(t)})^\dagger$, and $\tilde{\mathbf{S}} = \mathbf{C} \mathbf{W} \mathbf{C}^H$ is an approximation to \mathbf{S} . Let $\tilde{\mathbf{U}}$ be the orthonormal basis of $\tilde{\mathbf{S}}$.

Theorem 2. Let the notation be defined in the above. Repeat the iteration projection for t ($t \geq 0$) times. Let $\delta \in (0, 1)$ be any constant. The following relation holds with probability at least $1 - \delta$:

$$\sqrt{\frac{P_{\text{music}}(\theta)}{\tilde{P}_{\text{music}}(\theta)}} \leq 1 + \frac{\sqrt{M^2 K}}{\delta} \left(\frac{\sigma_{K+1}(\mathbf{S})}{\sigma_K(\mathbf{S})}\right)^{t+1}. \quad (19)$$

Theorem 2 establishes a lower bounds for $\tilde{P}_{\text{music}}(\theta)$ which is obtained via random projection in Section (III-B). The relative approximation error is basically

$$\mathcal{O}\left(\sqrt{M^2 K} \cdot \left(\frac{\sigma_{K+1}(\mathbf{S})}{\sigma_K(\mathbf{S})}\right)^{t+1}\right).$$

The approximation errors converge to zero exponentially with t . If the SNR is big, $\frac{\sigma_{K+1}(\mathbf{S})}{\sigma_K(\mathbf{S})}$ is very small; and therefore, our method converges to precise estimation in several iterations.

D. Upper Bound for Fast Method 2

Theorem 3. Let the notation be defined in Section IV-C. Repeat the iterative projection for t ($t \geq 0$) times. Then, with probability at least $1 - \delta$,

$$\sqrt{\frac{P_{\text{music}}(\theta)}{\tilde{P}_{\text{music}}(\theta)}} \geq 1 - \frac{\sqrt{M^2 K}}{\delta} \left(\frac{\sigma_{K+1}(\mathbf{S})}{\sigma_K(\mathbf{S})}\right)^{t+1}. \quad (20)$$

Theorem 3 establishes an upper bound for $\tilde{P}_{\text{music}}(\theta)$, which is also estimated via the random projection. Similarly, the relative approximation error is basically

$$\mathcal{O}\left(\sqrt{M^2 K} \cdot \left(\frac{\sigma_{K+1}(\mathbf{S})}{\sigma_K(\mathbf{S})}\right)^{t+1}\right).$$

It converges to zero exponentially. In particular, if the SNR is high, a few iterations will suffice for the high precision.

E. Accurate DoA Estimation

As shown latterly, in the context of massive-MIMO radars, the strong peaks of pseudo-spectrum, which are located exactly at target AoAs, are significantly higher than the noise baseline,

$$P_{\text{music}}(\theta_k) \gg P_0,$$

where $P_0 \triangleq \max \{P_{\text{music}}(\theta')\}$ denotes the maximum amplitude of non-target regions, i.e. $\theta' \notin \boldsymbol{\theta}_{K \times 1}$. Without losing generality, we assume it almost satisfies $P_{\text{music}}(\theta_k)/P_0 > \gamma$, when the SNR is not very small (e.g. $\gamma \sim M$, SNR=0dB, see the following Figure 7). When the approximated pseudo-spectrum misses one target peak located at θ_k , we must have

$$\sqrt{\tilde{P}_{\text{music}}(\theta_k)} \leq \sqrt{P_0}. \quad (21)$$

At the same time, according to our theoretical lower bounds in eq. (16), we are supposed to have

$$\frac{1}{1+\alpha_l} \sqrt{P_{\text{music}}(\theta_k)} \leq \sqrt{\tilde{P}_{\text{music}}(\theta_k)} \leq \sqrt{P_0},$$

and therefore,

$$\sqrt{\gamma} \leq \sqrt{P_{\text{music}}(\theta_k)/P_0} \leq 1 + \alpha_l. \quad (22)$$

On the other hand, according to the following numerical analysis (e.g. in Figure 5), we should have $1 + \alpha_l \rightarrow 1$ and

$$1 + \alpha_l < \sqrt{\gamma}. \quad (23)$$

By checking eq. (22) and (23), we conclude this contradiction result suggests eq. (21) should be invalid. I.e., the approximated pseudo-spectrum $\tilde{P}_{\text{music}}(\theta)$ should not miss the true peaks of targets. Similarly, from the upper bound in eq. (16), we can show the approximated pseudo-spectrum $\tilde{P}_{\text{music}}(\theta)$ should not mistake the non-target AoA as a target peak, which prevents the false alarm in automotive sensing.

V. NUMERICAL SIMULATION & ANALYSIS

In the section, we examine our fast-MUSIC methods via comprehensive numerical simulations, and meanwhile compare them with existing subspace algorithms in high-resolution AoAs estimation with massive-MIMO radars.

A. Experiment Settings

Since we are interested in the subspace separation as well as the AoA estimation, we directly start from a signal matrix \mathbf{Y} of M receiving elements. When it comes to the time complexity, we implement our fast-MUSIC methods in MATLAB. Since there is no loop or recursion in our new schemes, its efficiency can be fairly measured by the CPU runtime (CPU 2.59GHz, 32GB memory), which is proportional to the required number of multiplication flops. The averaged runtime is thus reported based on 100 independent realizations.

B. Complexity vs Accuracy

We compare the runtime of current subspace methods in obtaining high-resolution AoAs. Figure 4 shows the computing latency (seconds) against the number of antenna elements, M . We set $N = M$ and $K = 10$ in this numerical analysis. For

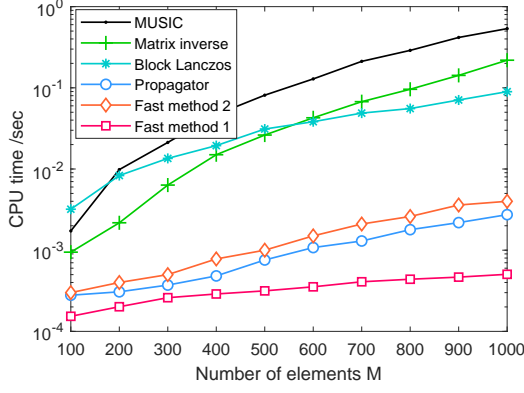


Fig. 4. Wall-clock runtime (second) against the number of antennas, M . We calculate only the runtime for computing the signal subspace which is the major bottleneck in automotive radar. Here we set $N = M$ and SNR = 0 dB.

our fast-MUSIC method 1, we configure $p = 12$. In our fast-MUSIC method 2, we have $t = 2$ and $p = 12$.

Despite the near-optimal accuracy in high-resolution environment sensing, the standard MUSIC unfortunately has $\mathcal{O}(M^3)$ time complexity, due to the computational SVD of a large covariance \mathbf{S} . As M increase, it easily becomes impractical for the real-time automotive scenarios, by producing an intolerable latency. When $M = 1000$, the latency of SVD alone consumes more than 500 milliseconds (ms), which is too much for real-time sensing application like unmanned aircrafts/vehicles. Here, we do not compare the other ESPRIT method, as it relies also on the exact SVD and has exactly the same runtime as MUSIC in the subspace extraction step.

Since the matrix inverse is somewhat more efficient than SVD, the subspace approximation method in [30] would be faster than MUSIC. But, it still requires a high complexity $\mathcal{O}\{M^3\}$, which may be unsuitable for real-time target estimation with massive-MIMO radars. In contrast, the well-known Lanczos method would reduce the time complexity to $\mathcal{O}\{KM^2\}$, which is more preferable to a standard MUSIC and a matrix-inverse method in large M . As far as subspace methods are concerned, the Propagator algorithm is highly efficient for massive-MIMO radars. However, as shown in later simulation, it would produce a less attractive accuracy.

By leveraging randomized matrix approximation, our fast-MUSIC method 1 relying on a uniform sampling is the most efficient, with its time complexity linearly scalable with M , i.e. $\mathcal{O}(p^2M)$ ($p \geq K$). As demonstrated in Figure 4, for a large antenna array $M = 1000$, our fast-MUSIC would be around 1000 times faster than the standard MUSIC. In this case, its required computation latency is only 0.5 ms (e.g. MUSIC consumes 500 ms). It is noteworthy that, although our fast method 2 theoretically has the complexity $\mathcal{O}(tpM^2)$, as previously discussed its real time cost is dramatically lower than the other block-Lanczos algorithm (since the involved matrix multiplication may be efficiently computed). This is further validated by the numerical results in Figure 4. As such, our fast method 2 is also applicable to real-time automotive sensing. E.g., its processing latency is 4 ms when $M = 1000$, slightly higher than a Propagator method (2.7 ms).

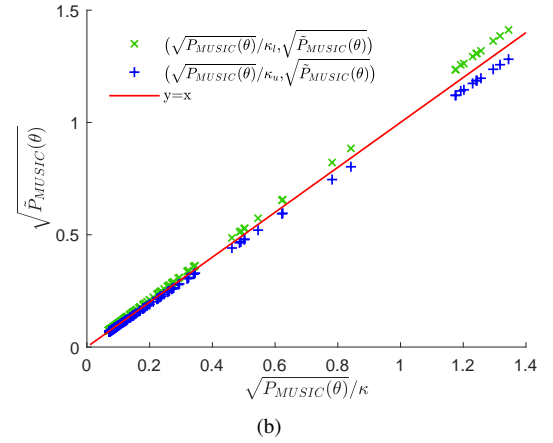
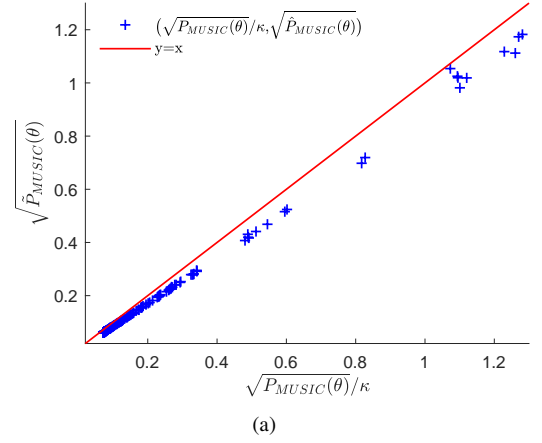


Fig. 5. Comparing the theoretical bounds (Theorems 1, 2, and 3) with the numerical results. (a) Theoretical bound of fast method 1. (b) Theoretical bounds of fast method 2, green cross – upper bound, blue cross – lower bound. The constants κ , κ_l , and κ_u are defined in Section V-C.

C. Error Bound vs Actual Error

We then study the accuracy of our theoretical error bounds (Theorems 1, 2, and 3), by comparing the pseudo-spectrum $\tilde{P}_{\text{music}}(\theta)$ approximated by fast-MUSIC with the exact one $P_{\text{music}}(\theta)$. In particular, we will show how much the bounds under-estimate or over-estimate an exact $P_{\text{music}}(\theta)$.

a) *Fast MUSIC – Method 1:* We first study the lower bound for the fast-MUSIC method 1, which is inspired by the random sampling. We denote the righthand side of the bound in Theorem 1 by $\kappa = 1 + \alpha_l$. Then, we have

$$\sqrt{\tilde{P}_{\text{music}}(\theta)} \geq \sqrt{P_{\text{music}}(\theta)}/\kappa \quad (24)$$

We repeat our numerical simulations to calculate a set of $\tilde{P}_{\text{music}}(\theta)$ and $P_{\text{music}}(\theta)$. In the numerical analysis, we configure $K = 11$, $M = N = 200$, $p = 12$ ³ and SNR=1dB.

In Figure 5(a), we plot $\sqrt{\tilde{P}_{\text{music}}(\theta)}/\kappa$ (the y -axis) against $\sqrt{\tilde{P}_{\text{music}}(\theta)}$ (the x -axis) as the blue crosses. Ideally, if the lower bound is tight ($\alpha_l \rightarrow 0$, $\kappa_l \rightarrow 1$), then the blue crosses should fall on the line $y = x$. Since the lower bound

³We assume $p = 10K \log(K)$ when deriving the theoretical lower bound. When implementing our fast method 1, we attain an accurate pseudo-spectrum, even a user-specific parameter is configured as $p \sim \mathcal{O}(K)$.

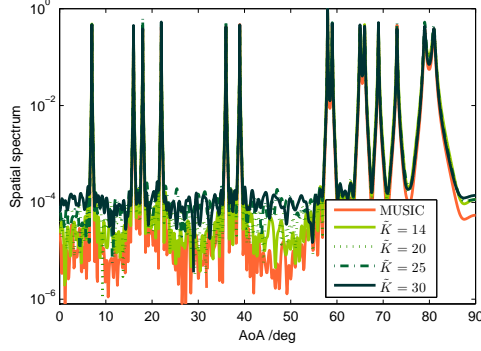


Fig. 6. Robustness of our fast MUSIC algorithm to inexact guess of K . Here, the actual number of targets is $K = 14$. The red curve plots MUSIC with the exact K . The other four curves plot our fast MUSIC algorithm with different guesses of K .

(righthand side of (24)) would under-estimate $\sqrt{\tilde{P}_{\text{music}}(\theta)}$, the blue crosses can fall below the line $y = x$ with the probability approaching 1. That means, our empirical results match the derived theoretical result, i.e., no blue cross is above $y = x$.

If θ' is in the non-target region ($\theta' \notin \theta_{K \times 1}$), then the pseudo-spectrum $P_{\text{music}}(\theta')$ is very small, $P_{\text{music}}(\theta') \sim \mathcal{O}(1/M)$. Figure 5(a) shows that our lower bound is very tight in the non-target region. As seen, the blue crosses are almost on the line $y = x$ and hence $\alpha_l \rightarrow 0$, e.g. $P_{\text{music}}(\theta') < 0.2$. Following our analysis, the approximated pseudo-spectrum $\tilde{P}_{\text{music}}(\theta')$ would not interpreted non-target AoAs as true peaks.

If θ_k is in the target region ($\theta_k \in \theta_{K \times 1}$), $P_{\text{music}}(\theta_k)$ is relatively large, $P_{\text{music}}(\theta_k) \sim 1$. Figure 5(a) shows that in the target region, the empirical results (blue cross) deviate slightly from the lower bound, indicating our lower bound is less tight in this region (e.g. $P_{\text{music}}(\theta_k) \sim 1$). However, this will be fine for realistic applications. I.e. $\tilde{P}_{\text{music}}(\theta_k)$ in the target regions is sufficiently large to detect the target AOA with the peaks, i.e. $1 + \alpha_l < 2 \ll \sqrt{\gamma}$.

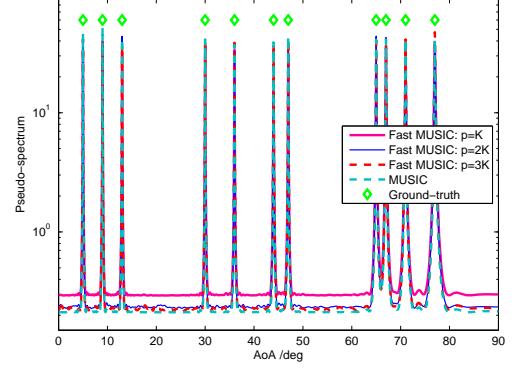
b) Fast MUSIC – Method 2: We then study the theoretical error bounds of our fast method 2, as in Theorems 2 and 3. We denote the righthand side of the lower bound in Theorem 2 by $\kappa_l = 1 + \alpha_l$; and the righthand side of the upper bound in Theorem 3 by $\kappa_u = 1 + \alpha_u$. Then, we expect

$$\sqrt{\tilde{P}_{\text{music}}(\theta)} \geq \sqrt{P_{\text{music}}(\theta)}/\kappa_l, \quad \sqrt{\tilde{P}_{\text{music}}(\theta)} \leq \sqrt{P_{\text{music}}(\theta)}/\kappa_u.$$

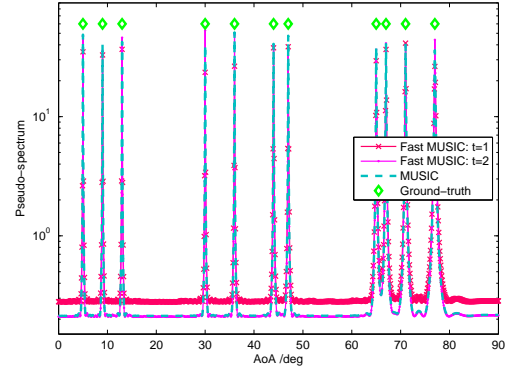
In the numerical analysis, we configure $K = 11$, $M = N = 200$, $p = 12$, $\delta = 0.2$ and $t = 2$. In Figure 5(b), we show $\sqrt{P_{\text{music}}(\theta)}/\kappa_l$ against $\sqrt{\tilde{P}_{\text{music}}(\theta)}$ as blue crosses, and $\sqrt{P_{\text{music}}(\theta)}/\kappa_u$ against $\sqrt{\tilde{P}_{\text{music}}(\theta)}$ as green crosses. As shown, the blue crosses and green crosses lie almost on the line $y = x$, indicating that our theoretical lower and upper bounds are very tight, i.e. $\alpha_l \rightarrow 0$ and $\alpha_u \rightarrow 0$. Combined with the theoretical analysis in Section IV-E, we thus conclude there is no false/missed peaks in our approximated pseudo-spectrum.

D. Robustness to Inaccurate K

As for the exact MUSIC, our fast-MUSIC methods need also the *a priori* knowledge of the number of targets, K , as the



(a) Pseudo-spectrum of the Nyström method with different p .



(b) Pseudo-spectrum of the power method with different t .

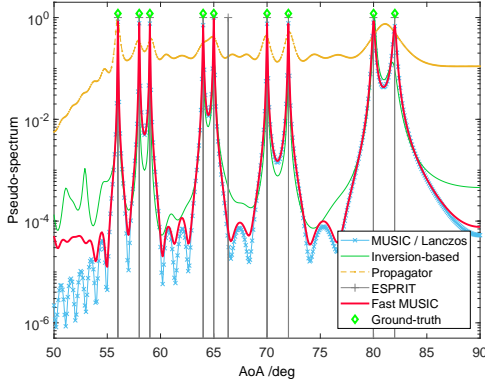
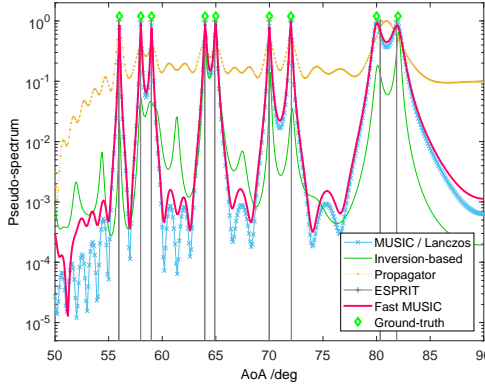
Fig. 7. We plot the pseudo-spectra of standard MUSIC and the fast-MUSIC methods with different tuning parameters.

dimension of the signal subspace. Unfortunately, in practice K is usually unknown beforehand. Thus, we have to use an estimate of K as the input of our fast-MUSIC.

In Figure 6, we study the effects on the approximated pseudo-spectrum from an inexact guess of K . In this analysis, we set $M = 200$, $N = 400$, $K = 14$, $\text{SNR} = 0$ dB, and $p = \text{round}(1.2 \times \hat{K})$. Here, the exact MUSIC is assumed with the exact knowledge, i.e. $K = 14$. As in Figure 6, our fast MUSIC method 1 is practically robust to an inexact guess of K . To be specific, when the guess value \hat{K} is larger than K , then our fast-MUSIC would produce almost the same pseudo-spectrum (especially at the peaks.)

E. Tuning Parameters

The fast-MUSIC method 1 (Algorithm 1) involves a key user-specific parameter p ($p \geq K$), which is used for trading off the accuracy and the complexity. That is to say, a large p is necessary to attain the tighter error bound (as in Theorem 1), which in turns increases the time complexity. Likewise, the fast-MUSIC method 2 (Algorithm 2) contains also one tuning parameter t ($t \geq 1$). In the following analysis, we will discuss the practical settings of p or t . Here, we fix $M = N = 200$, $K = 11$, and $\text{SNR} = 0$ dB.

(a) $M = 200$, $N = 800$, and $\text{SNR} = 0$ dB.(b) $M = N = 200$ and $\text{SNR} = 0$ dB.Fig. 8. Estimated pseudo-spectrum $\tilde{P}(\theta)$ of various algorithms. Here, the proposed algorithm refers to the fast-MUSIC method with $p = 12$.

In Figure 7(a), we plot the approximated pseudo-spectrum of our fast MUSIC under different settings of p . We find that, under all the three settings ($p = K$, $2K$, and $3K$), the fast algorithm successfully obtains the accurate AoA estimation of K targets. Define the approximation error between such two pseudo-spectrum as $\sum_{l=0}^{L-1} [\tilde{P}_{\text{music}}(\theta_l) - P_{\text{music}}(\theta_l)]^2$. When p is increased from K to $2K$, then the error drops from 0.59 to 0.11; when p is further increased to $3K$, then the approximation error would be marginal.

In Figure 7(b), we show the approximated pseudo-spectrum of our fast method 2 under different settings of t ($P = K$). We find that, with $t = 2$, the approximation error is 0.03, which is sufficiently small for the accurate AoAs estimation. In real-world automotive sensing, we may use $t = 2$ to approximate the MUSIC pseudo-spectrum via our fast method 2.

F. Accuracy in AoA Estimation

We then evaluate the AoA estimation accuracy and compare our fast-MUSIC with the existing subspace algorithms. In Figure 8, the normalized pseudo-spectrum is defined as:

$$\tilde{P}(\theta) = \frac{P(\theta) - \min_{\theta} \{P(\theta)\}}{\max_{\theta} \{P(\theta)\} - \min_{\theta} \{P(\theta)\}}$$

where $P(\theta)$ can be the spectrum of MUSIC, ESPRIT, Propagator, etc. In our numerical simulations, we configure $M = 200$ and $K = 9$ and then evaluate the relative accuracy under

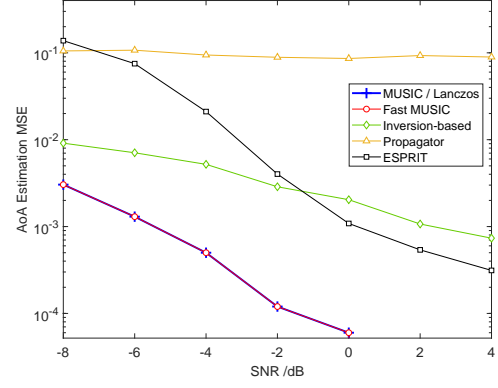


Fig. 9. Plot of AoA estimation MSE against SNRs.

different N . Here, we focus on our fast-MUSIC method 1 in which we assume $p = 12$.

As shown in Figure 8, among all these compared algorithms, both MUSIC and block-Lanczos algorithms attain the near-optimal pseudo-spectrum by exploiting the exact subspace information, which hence acquire the highly accurate AoAs estimation. Our fast-MUSIC obtains an approximated pseudo-spectrum that closely tracks the exact MUSIC. Moreover, the pseudo-spectrum of both MUSIC and our fast-MUSIC will not change, when the sample length N drops from $N = 800$ to $N = 200$. In comparison, another ESPRIT method obtains the less accurate AoAs estimation. The unexpected error (i.e. false targets nearby 65 degrees) seems to be inevitable, especially when the exact number of sources (i.e. K) remains unknown as in many applications.

Despite a low time complexity, the Propagator method produces a less accurate pseudo-spectrum. For one thing, the fluctuated baseline is relatively high, which may arouse false objects in low SNR cases. For another, as one inherent disadvantage, it gets the low resolution results when unknown DoAs surpass 70 degree. For example, it may misinterpret two targets (between 80 and 85 degrees) as one fake object, resulting in significant estimation errors. Note that, the modified Propagator algorithm has been proposed to improve the accuracy [28], which, however, requires a special array structure (e.g. L -shape array) and may be less attractive for compact MIMO radar (i.e. deployed on a front bumper of car).

For another matrix-inversion method, although its time complexity in approximating a noise subspace is reduced to some extents, it still has two drawbacks in real applications. First, in order to accurately estimating AoAs, the required sample length N would be relatively large. Second, its estimation accuracy may be guaranteed only in the condition of high SNRs, so that the approximated subspace is sufficiently accurate (as discussed in Section II-B). In the case of a short length $N \leq M$ or a strong noise ($\sigma_K(\mathbf{S}) \simeq \sigma_n^2$), it becomes unstable and produces false objects or inaccurate AoAs.

Except for the linear scalability and the real-time implementation, our fast-MUSIC is highly accurate and stable, as shown in Figure 8. Unlike its counterparts that have to sacrifice accuracy for complexity, this new approach overcomes the long-standing contradiction between high resolution and low

complexity. By achieving the high-resolution estimation at a linear scalable complexity, it provides the great potential to future massive-MIMO radars, especially for the emerging automotive scenarios with one ambitious goal – the real-time super-resolution sensing.

G. Performance under Varying SNRs

We finally evaluate the AoA estimation errors of various methods in the context of massive-MIMO radar. The mean square error (MSE) of estimated AoAs is measured by:

$$\text{MSE} \triangleq \mathbb{E} \left\{ \sum_{k=1}^K \|\theta_k - \hat{\theta}_k\|_2^2 \right\}. \quad (25)$$

Here, θ_k denotes the ground truth AoA of the k th target point, whilst $\hat{\theta}_k$ is the derived estimation. In Figure 9, we show the MSE performance of existing subspace methods. The AoA estimation MSE of all subspace methods would be reduced, as the SNR increases. As expected, our fast-MUSIC attains the same MSEs as the standard MUSIC. In other words, our new approach sacrifices no estimation accuracy and attains the high-resolution AoA estimations.

VI. CONCLUSION

We investigate the high-resolution target estimation problem emerging from automotive massive-MIMO radar. Existing popular subspace methods (e.g. MUSIC and ESPRIT) are computationally expensive, due to the complex decomposition of a large covariance matrix. Other approximation schemes, e.g. matrix-inverse and propagator methods, lead to the degraded accuracy. As one long-standing problem in MIMO signal processing, the high-resolution estimation and real-time computation remain mutually exclusive.

To enable real-time yet super-resolution target estimation/detection, we leverage randomized matrix approximation and develop two fast-MUSIC algorithms, whereby a large covariance is approximated by small sketches that are abstracted via random sampling / projection. We theoretically proved that in the case of high SNRs, our fast-MUSIC is almost as good as the near-optimal standard MUSIC. Our numerical study further demonstrates that, while our new approaches are faster dramatically than a standard MUSIC by orders-of-magnitude, they are nearly as accurate as MUSIC in acquiring AoA estimations. So, our fast-MUSIC enjoys both linear complexity and high accuracy, breaking the theoretical bottleneck in MIMO radar processing. It would provide the great potential to high-resolution and real-time massive-MIMO radars in emerging automotive applications.

APPENDIX

Here, we show the detailed proofs of Theorems 1, 2, and 3. For simplicity, we leave out the θ in $P_{\text{music}}(\theta)$, $\tilde{P}_{\text{music}}(\theta)$, and $\mathbf{a}(\theta)$.

A. Analysis of Uniform Sampling

An $M \times p$ ($p < M$) matrix $\mathbf{\Pi}$ is called a uniform sampling matrix if its columns are sampled from the columns

of $\frac{\sqrt{M}}{\sqrt{p}} \mathbf{I}_M$ uniformly at random. For any $N \times M$ matrix \mathbf{X} , the multiplication $\mathbf{X}\mathbf{\Pi}$ ($N \times p$) contains p uniformly sampled columns of \mathbf{X} .

Lemma 1. Let $\mathbf{\Pi}$ be an $M \times p$ uniform sampling matrix. Then

$$\|\mathbf{\Pi}\|_2^2 = M/p.$$

Lemma 2 ([45], [48]). Let \mathbf{U}_K be an $M \times K$ matrix with orthonormal columns. Let the row coherence of \mathbf{U}_K be defined as $\mu(\mathbf{U}_K) = \frac{M}{K} \max_i \|(\mathbf{U}_K)_i\|_2^2 \in [1, \frac{M}{K}]$. Let $\mathbf{\Pi}$ be an $M \times p$ uniform sampling matrix. For

$$p \geq \frac{(6 + 2\eta)\mu(\mathbf{U}_K)K}{3\eta^2} \log \frac{K}{\delta}$$

the K singular values of $\mathbf{U}_K^H \mathbf{\Pi} \mathbf{\Pi}^H \mathbf{U}_K$ are at least $1 - \eta$ with probability at least $1 - \delta$.

B. Analysis of Gaussian Projection

Lemma 3 ([49]). Let $\mathbf{\Pi}$ be an $M \times K$ matrix whose entries are i.i.d. drawn from $\mathcal{N}(0, 1)$. If M is substantially larger than K , the spectral norm of $\mathbf{\Pi}$ is bounded by

$$\|\mathbf{\Pi}\|_2 \leq \sqrt{M} + \sqrt{K} + \mathcal{O}(1), \quad \text{almost surely.}$$

Lemma 4 ([50], [51]). Let \mathbf{G} be a $K \times K$ matrix whose entries are i.i.d. drawn from $\mathcal{N}(0, 1)$. Then the smallest singular value of \mathbf{G} satisfies

$$\sigma_K(\mathbf{G}) \geq \frac{\delta}{\sqrt{K}}$$

with probability at least $1 - \delta - o(1)$.

C. Proof of Theorem 1

Lemma 5. Let the notation be defined in Section IV-B. Let $\mathbf{\Pi}$ be any matrix with $\text{rank}(\mathbf{U}_K^H \mathbf{\Pi}) \geq K$. Then, for all \mathbf{a} ,

$$\begin{aligned} & \|\mathbf{U}_K \mathbf{U}_K^H \mathbf{a} - \tilde{\mathbf{U}} \tilde{\mathbf{U}}^H \mathbf{U}_K \mathbf{U}_K^H \mathbf{a}\|_2 \\ & \leq \|(\mathbf{S} - \mathbf{S}_K) \mathbf{\Pi} (\mathbf{U}_K^H \mathbf{\Pi})^\dagger \Sigma_K^{-1} \mathbf{U}_K^H \mathbf{a}\|_2, \end{aligned}$$

Proof. Let $\tilde{\mathbf{U}}$ be the orthonormal bases of $\tilde{\mathbf{S}}$. Lemma 12 of [48] shows that

$$(\mathbf{C} \mathbf{W}^\dagger \mathbf{C}^H) (\mathbf{C} \mathbf{W}^\dagger \mathbf{C}^H)^\dagger \mathbf{C} = \mathbf{C}.$$

Thus $\mathbf{C} = \mathbf{S} \mathbf{\Pi}$ is in the subspace spanned by the columns of $\tilde{\mathbf{U}}$, and therefore,

$$\tilde{\mathbf{U}} \tilde{\mathbf{U}}^H \mathbf{S} \mathbf{\Pi} = \mathbf{S} \mathbf{\Pi}. \quad (26)$$

It is not hard to prove that

$$\tilde{\mathbf{U}}^H \mathbf{U}_K \mathbf{U}_K^H \mathbf{a} = \underset{\mathbf{x}}{\text{argmin}} \|\mathbf{U}_K \mathbf{U}_K^H \mathbf{a} - \tilde{\mathbf{U}} \mathbf{x}\|_2.$$

Thus, the inequality holds for all $\tilde{\mathbf{x}}$:

$$\begin{aligned} & \|\mathbf{U}_K \mathbf{U}_K^H \mathbf{a} - \tilde{\mathbf{U}} \tilde{\mathbf{U}}^H \mathbf{U}_K \mathbf{U}_K^H \mathbf{a}\|_2 \\ & = \min_{\mathbf{x}} \|\mathbf{U}_K \mathbf{U}_K^H \mathbf{a} - \tilde{\mathbf{U}} \mathbf{x}\|_2 \leq \|\mathbf{U}_K \mathbf{U}_K^H \mathbf{a} - \tilde{\mathbf{U}} \tilde{\mathbf{x}}\|_2. \end{aligned} \quad (27)$$

We artificially construct

$$\tilde{\mathbf{x}} = \tilde{\mathbf{U}}^H \mathbf{S} \mathbf{\Pi} (\mathbf{U}_K^H \mathbf{\Pi})^\dagger \Sigma_K^{-1} \mathbf{U}_K^H \mathbf{a}.$$

It follows from (26) that

$$\begin{aligned}\tilde{\mathbf{U}}\tilde{\mathbf{x}} &= \tilde{\mathbf{U}}\tilde{\mathbf{U}}^H\mathbf{S}\Pi(\mathbf{U}_K^H\Pi)^\dagger\Sigma_K^{-1}\mathbf{U}_K^H\mathbf{a} \\ &= \mathbf{S}\Pi(\mathbf{U}_K^H\Pi)^\dagger\Sigma_K^{-1}\mathbf{U}_K^H\mathbf{a} \\ &= (\mathbf{S}_K + \mathbf{S} - \mathbf{S}_K)\Pi(\mathbf{U}_K^H\Pi)^\dagger\Sigma_K^{-1}\mathbf{U}_K^H\mathbf{a}.\end{aligned}\quad (28)$$

Since $\text{rank}(\mathbf{U}_K^H\Pi) \geq K$, we have $(\mathbf{U}_K^H\Pi)(\mathbf{U}_K^H\Pi)^\dagger = \mathbf{I}_K$. Thus

$$\begin{aligned}\mathbf{S}_K\Pi(\mathbf{U}_K^H\Pi)^\dagger\Sigma_K^{-1}\mathbf{U}_K\mathbf{a} \\ &= \mathbf{U}_K\Sigma_K\mathbf{U}_K^H\Pi(\mathbf{U}_K^H\Pi)^\dagger\Sigma_K^{-1}\mathbf{U}_K^H\mathbf{a} \\ &= \mathbf{U}_K\Sigma_K\Sigma_K^{-1}\mathbf{U}_K^H\mathbf{a} = \mathbf{U}_K\mathbf{U}_K^H\mathbf{a}.\end{aligned}\quad (29)$$

It follows from (28) and (29) that

$$\begin{aligned}\tilde{\mathbf{U}}\tilde{\mathbf{x}} &= [\mathbf{S}_K + (\mathbf{S} - \mathbf{S}_K)]\Pi(\mathbf{U}_K^H\Pi)^\dagger\Sigma_K^{-1}\mathbf{U}_K^H\mathbf{a} \\ &= \mathbf{U}_K\mathbf{U}_K^H\mathbf{a} + (\mathbf{S} - \mathbf{S}_K)\Pi(\mathbf{U}_K^H\Pi)^\dagger\Sigma_K^{-1}\mathbf{U}_K^H\mathbf{a}.\end{aligned}\quad (30)$$

It follows from (27) and (30) that

$$\begin{aligned}\|\mathbf{U}_K\mathbf{U}_K^H\mathbf{a} - \tilde{\mathbf{U}}\tilde{\mathbf{U}}^H\mathbf{U}_K\mathbf{U}_K^H\mathbf{a}\|_2 &\leq \|\mathbf{U}_K\mathbf{U}_K^H\mathbf{a} - \tilde{\mathbf{U}}\tilde{\mathbf{x}}\|_2 \\ &= \|(\mathbf{S} - \mathbf{S}_K)\Pi(\mathbf{U}_K^H\Pi)^\dagger\Sigma_K^{-1}\mathbf{U}_K^H\mathbf{a}\|_2,\end{aligned}$$

by which the lemma follows. \square

Complete the proof of Theorem 1:

Proof. The $M \times p$ matrix Π is a uniform sampling matrix. Then $\mathbf{C} = \mathbf{S}\Pi$ and $\mathbf{W} = \Pi^T\mathbf{S}\Pi$. Lemma 1 shows the spectral norm of Π is bounded by

$$\|\Pi\|_2 \leq \sqrt{M/p}.$$

Because \mathbf{U}_K has orthonormal columns, Lemma 2 shows that for $p \geq \frac{(6+2\eta)\mu(\mathbf{U}_K)K}{3\eta^2} \log \frac{K}{\delta}$, the K -th singular value of $\mathbf{U}_K^H\Pi$ is bounded by

$$\sigma_K(\mathbf{U}_K^H\Pi) \geq \sqrt{1-\eta}$$

with probability at least $1 - \delta$. Let follows from Lemma 5 that

$$\begin{aligned}\|(\mathbf{I}_M - \tilde{\mathbf{U}}\tilde{\mathbf{U}}^H)\mathbf{U}_K\mathbf{U}_K^H\mathbf{a}\|_2 \\ &\leq \|\mathbf{U}_K\mathbf{U}_K^H\mathbf{a} - \tilde{\mathbf{U}}\tilde{\mathbf{U}}^H\mathbf{U}_K\mathbf{U}_K^H\mathbf{a}\|_2 \\ &\leq \|(\mathbf{S} - \mathbf{S}_K)\Pi(\mathbf{U}_K^H\Pi)^\dagger\Sigma_K^{-1}\mathbf{U}_K^H\mathbf{a}\|_2 \\ &\leq \|(\mathbf{S} - \mathbf{S}_K)\|_2 \|\Pi\|_2 \|(\mathbf{U}_K^H\Pi)^\dagger\|_2 \|\Sigma_K^{-1}\|_2 \|\mathbf{U}_K^H\mathbf{a}\|_2 \\ &\leq \frac{\sigma_{K+1}(\mathbf{S})}{\sigma_K(\mathbf{S})} \frac{\sqrt{M/p}}{\sqrt{1-\eta}} \|\mathbf{U}_K^H\mathbf{a}\|_2.\end{aligned}$$

We set $\eta = 0.75$. Then, for

$$p \geq 4.5\mu(\mathbf{U}_K)K \cdot \log \frac{K}{\delta},$$

it holds with probability at least $1 - \delta$ that

$$\|(\mathbf{I}_M - \tilde{\mathbf{U}}\tilde{\mathbf{U}}^H)\mathbf{U}_K\mathbf{U}_K^H\mathbf{a}\|_2 \leq 2\sqrt{\frac{M}{p}} \frac{\sigma_{K+1}(\mathbf{S})}{\sigma_K(\mathbf{S})} \|\mathbf{U}_K^H\mathbf{a}\|_2.$$

It follows that

$$\begin{aligned}\|(\mathbf{I}_M - \tilde{\mathbf{U}}\tilde{\mathbf{U}}^H)\mathbf{a}\|_2 \\ &= \|(\mathbf{I}_M - \tilde{\mathbf{U}}\tilde{\mathbf{U}}^H)(\mathbf{U}_K\mathbf{U}_K^H + \mathbf{U}_{-K}\mathbf{U}_{-K}^H)\mathbf{a}\|_2 \\ &\leq \|(\mathbf{I}_M - \tilde{\mathbf{U}}\tilde{\mathbf{U}}^H)\mathbf{U}_K\mathbf{U}_K^H\mathbf{a}\|_2 + \|\mathbf{U}_{-K}\mathbf{U}_{-K}^H\mathbf{a}\|_2.\end{aligned}$$

Hence,

$$\begin{aligned}\|(\mathbf{I}_M - \tilde{\mathbf{U}}\tilde{\mathbf{U}}^H)\mathbf{a}\|_2 - \|(\mathbf{I}_M - \mathbf{U}_K\mathbf{U}_K^H)\mathbf{a}\|_2 \\ \leq \|(\mathbf{I}_M - \tilde{\mathbf{U}}\tilde{\mathbf{U}}^H)\mathbf{U}_K\mathbf{U}_K^H\mathbf{a}\|_2 \leq 2\sqrt{\frac{M}{p}} \frac{\sigma_{K+1}(\mathbf{S})}{\sigma_K(\mathbf{S})} \|\mathbf{U}_K^H\mathbf{a}\|_2,\end{aligned}$$

where the last inequality holds with probability at least $1 - \delta$.

We leave out θ in $P_{\text{music}}(\theta)$, $\tilde{P}_{\text{music}}(\theta)$, and $\mathbf{a}(\theta)$. It follows from (8) and (14) that

$$\begin{aligned}\sqrt{\frac{P_{\text{music}}}{\tilde{P}_{\text{music}}}} &= \frac{\|(\mathbf{I} - \tilde{\mathbf{U}}\tilde{\mathbf{U}}^H)\mathbf{a}\|_2}{\|(\mathbf{I} - \mathbf{U}_K\mathbf{U}_K^H)\mathbf{a}\|_2} \\ &\leq 1 + 2\sqrt{\frac{M}{p}} \frac{\sigma_{K+1}(\mathbf{S})}{\sigma_K(\mathbf{S})} \frac{\|\mathbf{U}_K^H\mathbf{a}\|_2}{\|(\mathbf{I} - \mathbf{U}_K\mathbf{U}_K^H)\mathbf{a}\|_2}.\end{aligned}$$

Furthermore, when the number of element is sufficiently large, for an variant pseudo-spectrum spectrum $\|\mathbf{U}_K^H\mathbf{a}\|_2$ and $\|(\mathbf{I} - \mathbf{U}_K\mathbf{U}_K^H)\mathbf{a}\|_2$, the following relations always hold:

$$\|\mathbf{U}_K^H\mathbf{a}\|_2^2 \leq \|\mathbf{U}_K^H\mathbf{a}(\theta_k)\|_2^2 \rightarrow M, \quad (31)$$

and

$$\|(\mathbf{I} - \mathbf{U}_K\mathbf{U}_K^H)\mathbf{a}\|_2 \geq \|(\mathbf{I} - \mathbf{U}_K\mathbf{U}_K^H)\mathbf{a}(\theta_k)\|_2 \rightarrow 1, \quad (32)$$

where θ_k denotes the k -th AoA of target point. As a result, we further have:

$$\frac{\|\mathbf{U}_K^H\mathbf{a}\|_2}{\|(\mathbf{I} - \mathbf{U}_K\mathbf{U}_K^H)\mathbf{a}\|_2} \leq \frac{\|\mathbf{U}_K^H\mathbf{a}\|_2}{\|\mathbf{a}\|_2} \leq \sqrt{M}. \quad (33)$$

On this basis, we can finally obtain the Theorem 1:

$$\sqrt{\frac{P_{\text{music}}}{\tilde{P}_{\text{music}}}} \leq 1 + 2\sqrt{\frac{M^2}{p}} \frac{\sigma_{K+1}(\mathbf{S})}{\sigma_K(\mathbf{S})}.$$

\square

D. Proof of Theorem 2

Lemma 6. Let the notation be defined in Section IV-C. Let Π be any matrix satisfying that $\text{rank}(\mathbf{U}_K^H\Pi) \geq K$. Then, for all \mathbf{a} ,

$$\begin{aligned}\|\mathbf{U}_K\mathbf{U}_K^H\mathbf{a} - \tilde{\mathbf{U}}\tilde{\mathbf{U}}^H\mathbf{U}_K\mathbf{U}_K^H\mathbf{a}\|_2 \\ \leq \|(\mathbf{S} - \mathbf{S}_K)^{t+1}\Pi(\mathbf{U}_K^H\Pi)^\dagger\Sigma_K^{-t-1}\mathbf{U}_K^H\mathbf{a}\|_2.\end{aligned}$$

Proof. Since $\tilde{\mathbf{S}} = \mathbf{C}\mathbf{W}^\dagger\mathbf{C}^H$, it follows from [48, Lemma 12] that

$$\tilde{\mathbf{S}}\tilde{\mathbf{S}}^\dagger\mathbf{C} = \mathbf{C}.$$

Since $\tilde{\mathbf{U}}$ is an orthonormal bases of $\tilde{\mathbf{S}}$,

$$\tilde{\mathbf{U}}\tilde{\mathbf{U}}^H\mathbf{C} = \tilde{\mathbf{S}}\tilde{\mathbf{S}}^\dagger\mathbf{C} = \mathbf{C}.$$

By the definition $\mathbf{C} = \mathbf{S}\mathbf{V}$ and that \mathbf{V} is the orthonormal basis of $\mathbf{S}^t\Pi$, we have that \mathbf{C} and $\mathbf{S}^{t+1}\Pi$ have the same column space.

$$\tilde{\mathbf{U}}\tilde{\mathbf{U}}^H\mathbf{S}^{t+1}\Pi = \mathbf{S}^{t+1}\Pi. \quad (34)$$

In the same way as the proof of Lemma 5, we can prove that for all $\tilde{\mathbf{x}}$:

$$\|\mathbf{U}_K\mathbf{U}_K^H\mathbf{a} - \tilde{\mathbf{U}}\tilde{\mathbf{U}}^H\mathbf{U}_K\mathbf{U}_K^H\mathbf{a}\|_2 \leq \|\mathbf{U}_K\mathbf{U}_K^H\mathbf{a} - \tilde{\mathbf{U}}\tilde{\mathbf{x}}\|_2. \quad (35)$$

We artificially construct □

$$\tilde{\mathbf{x}} = \tilde{\mathbf{U}}^H \mathbf{S}^{t+1} \mathbf{\Pi} (\mathbf{U}_K^H \mathbf{\Pi})^\dagger \Sigma_K^{-t-1} \mathbf{U}_K^H \mathbf{a}.$$

It follows from (34) that

$$\begin{aligned} \tilde{\mathbf{U}} \tilde{\mathbf{x}} &= \tilde{\mathbf{U}} \tilde{\mathbf{U}}^H \mathbf{S}^{t+1} \mathbf{\Pi} (\mathbf{U}_K^H \mathbf{\Pi})^\dagger \Sigma_K^{-t-1} \mathbf{U}_K^H \mathbf{a} \\ &= (\mathbf{S}_K^{t+1} + \mathbf{S}^{t+1} - \mathbf{S}_K^{t+1}) \mathbf{\Pi} (\mathbf{U}_K^H \mathbf{\Pi})^\dagger \Sigma_K^{-t-1} \mathbf{U}_K^H \mathbf{a}. \end{aligned} \quad (36)$$

In the same way as the proof of Lemma 5, we can use $\text{rank}(\mathbf{U}_K^H \mathbf{\Pi}) \geq K$ to show that

$$\begin{aligned} &\mathbf{S}_K^{t+1} \mathbf{\Pi} (\mathbf{U}_K^H \mathbf{\Pi})^\dagger \Sigma_K^{-t-1} \mathbf{U}_K^H \mathbf{a} \\ &= \mathbf{U}_K \Sigma_K^{t+1} \mathbf{U}_K^H \mathbf{\Pi} (\mathbf{U}_K^H \mathbf{\Pi})^\dagger \Sigma_K^{-t-1} \mathbf{U}_K^H \mathbf{a} \\ &= \mathbf{U}_K \Sigma_K^{t+1} \Sigma_K^{-t-1} \mathbf{U}_K^H \mathbf{a} = \mathbf{U}_K \mathbf{U}_K^H \mathbf{a}. \end{aligned}$$

It follows from (36) that

$$\tilde{\mathbf{U}} \tilde{\mathbf{x}} = \mathbf{U}_K \mathbf{U}_K^H \mathbf{a} + (\mathbf{S}^{t+1} - \mathbf{S}_K^{t+1}) \mathbf{\Pi} (\mathbf{U}_K^H \mathbf{\Pi})^\dagger \Sigma_K^{-t-1} \mathbf{U}_K^H \mathbf{a}.$$

It follows from (35) that

$$\begin{aligned} &\|\mathbf{U}_K \mathbf{U}_K^H \mathbf{a} - \tilde{\mathbf{U}} \tilde{\mathbf{U}}^H \mathbf{U}_K \mathbf{U}_K^H \mathbf{a}\|_2 \\ &\leq \|(\mathbf{S}^{t+1} - \mathbf{S}_K^{t+1}) \mathbf{\Pi} (\mathbf{U}_K^H \mathbf{\Pi})^\dagger \Sigma_K^{-t-1} \mathbf{U}_K^H \mathbf{a}\|_2, \end{aligned}$$

by which the lemma follows. □

Complete the proof of Theorem 2:

Proof. Lemma 3 shows that the spectral norm of the $M \times K$ standard Gaussian matrix $\mathbf{\Pi}$ satisfies

$$\|\mathbf{\Pi}\|_2 \leq \sqrt{M} + \sqrt{K} + \mathcal{O}(1), \quad \text{almost surely.}$$

Since \mathbf{U}_K has orthonormal columns, the $K \times K$ matrix $\mathbf{U}_K^H \mathbf{\Pi}$ is a standard Gaussian matrix. It follows from Lemma 4 that

$$\sigma_K^{-1}(\mathbf{U}_K^H \mathbf{\Pi}) \leq \frac{\sqrt{K}}{\delta}$$

with probability at least $1 - \delta - o(1)$. It follows from Lemma 6 that

$$\begin{aligned} &\|\mathbf{U}_K \mathbf{U}_K^H \mathbf{a} - \tilde{\mathbf{U}} \tilde{\mathbf{U}}^H \mathbf{U}_K \mathbf{U}_K^H \mathbf{a}\|_2 \\ &\leq \|(\mathbf{S}^{t+1} - \mathbf{S}_K^{t+1}) \mathbf{\Pi} (\mathbf{U}_K^H \mathbf{\Pi})^\dagger \Sigma_K^{-t-1} \mathbf{U}_K^H \mathbf{a}\|_2 \\ &\leq \left(\frac{\sigma_{K+1}(\mathbf{S})}{\sigma_K(\mathbf{S})}\right)^{t+1} \|\mathbf{\Pi}\|_2 \|(\mathbf{U}_K^H \mathbf{\Pi})^\dagger\|_2 \|\mathbf{U}_K^H \mathbf{a}\|_2 \\ &\leq \left(\frac{\sigma_{K+1}(\mathbf{S})}{\sigma_K(\mathbf{S})}\right)^{t+1} \frac{\sqrt{MK} + K + \mathcal{O}(\sqrt{K})}{\delta} \|\mathbf{U}_K^H \mathbf{a}\|_2. \end{aligned}$$

The proof follows from the proof of Theorem 1 that

$$\sqrt{\frac{P_{\text{music}}}{\tilde{P}_{\text{music}}}} = \frac{\|(\mathbf{I} - \tilde{\mathbf{U}} \tilde{\mathbf{U}}^H) \mathbf{a}\|_2}{\|(\mathbf{I} - \mathbf{U}_K \mathbf{U}_K^H) \mathbf{a}\|_2} \leq 1 + \frac{\|(\mathbf{I} - \tilde{\mathbf{U}} \tilde{\mathbf{U}}^H) \mathbf{U}_K \mathbf{U}_K^H \mathbf{a}\|_2}{\|(\mathbf{I} - \mathbf{U}_K \mathbf{U}_K^H) \mathbf{a}\|_2}.$$

Thus, it holds with probability at least $1 - \delta - o(1)$ that

$$\sqrt{\frac{P_{\text{music}}}{\tilde{P}_{\text{music}}}} \leq 1 + \left(\frac{\sigma_{K+1}(\mathbf{S})}{\sigma_K(\mathbf{S})}\right)^{t+1} \frac{\sqrt{MK}(1+o(1))}{\delta} \frac{\|\mathbf{U}_K^H \mathbf{a}\|_2}{\|(\mathbf{I} - \mathbf{U}_K \mathbf{U}_K^H) \mathbf{a}\|_2},$$

by incorporating eq. (33), then the theorem can be proved, i.e.

$$\begin{aligned} \sqrt{\frac{P_{\text{music}}}{\tilde{P}_{\text{music}}}} &\leq 1 + \left(\frac{\sigma_{K+1}(\mathbf{S})}{\sigma_K(\mathbf{S})}\right)^{t+1} \frac{\sqrt{MK}(1+o(1))}{\delta} \sqrt{M}, \\ &= 1 + \frac{\sqrt{M^2 K}}{\delta} \left(\frac{\sigma_{K+1}(\mathbf{S})}{\sigma_K(\mathbf{S})}\right)^{t+1}. \end{aligned}$$

Proof of Theorem 3:

Proof. It can be shown that for all $\tilde{\mathbf{X}}$:

$$\|\mathbf{U}_K \mathbf{U}_K^H - \tilde{\mathbf{U}} \tilde{\mathbf{U}}^H \mathbf{U}_K \mathbf{U}_K^H\|_2 \leq \|\mathbf{U}_K \mathbf{U}_K^H - \tilde{\mathbf{U}} \tilde{\mathbf{X}}\|_2.$$

We artificially construct

$$\tilde{\mathbf{X}} = \tilde{\mathbf{U}}^H \mathbf{S}^{t+1} \mathbf{\Pi} (\mathbf{U}_K^H \mathbf{\Pi})^\dagger \Sigma_K^{-t-1} \mathbf{U}_K^H.$$

In the same way as the proof of Lemma 6, we can show that

$$\tilde{\mathbf{U}} \tilde{\mathbf{X}} = \mathbf{U}_K \mathbf{U}_K^H + (\mathbf{S}^{t+1} - \mathbf{S}_K^{t+1}) \mathbf{\Pi} (\mathbf{U}_K^H \mathbf{\Pi})^\dagger \Sigma_K^{-t-1} \mathbf{U}_K^H.$$

Thus

$$\begin{aligned} &\|\mathbf{U}_K \mathbf{U}_K^H - \tilde{\mathbf{U}} \tilde{\mathbf{U}}^H \mathbf{U}_K \mathbf{U}_K^H\|_2 \\ &\leq \|(\mathbf{S}^{t+1} - \mathbf{S}_K^{t+1}) \mathbf{\Pi} (\mathbf{U}_K^H \mathbf{\Pi})^\dagger \Sigma_K^{-t-1} \mathbf{U}_K^H\|_2 \\ &\leq \left(\frac{\sigma_{K+1}(\mathbf{S})}{\sigma_K(\mathbf{S})}\right)^{t+1} \|\mathbf{\Pi}\|_2 \|(\mathbf{U}_K^H \mathbf{\Pi})^\dagger\|_2. \end{aligned}$$

It follows from the proof of Theorem 2 that

$$\begin{aligned} &\|\mathbf{U}_K \mathbf{U}_K^H - \tilde{\mathbf{U}} \tilde{\mathbf{U}}^H \mathbf{U}_K \mathbf{U}_K^H\|_2 \\ &\leq [1 + o(1)] \frac{\sqrt{MK}}{\delta} \left(\frac{\sigma_{K+1}(\mathbf{S})}{\sigma_K(\mathbf{S})}\right)^{t+1} \end{aligned}$$

holds with probability at least $1 - \delta$. Since \mathbf{U}_K and $\tilde{\mathbf{U}}$ are both $M \times K$, [52, Eqn 2.54] shows that

$$\|(\mathbf{I}_M - \tilde{\mathbf{U}} \tilde{\mathbf{U}}^H) \mathbf{U}_K\|_2 = \|(\mathbf{I}_M - \mathbf{U}_K \mathbf{U}_K^H) \tilde{\mathbf{U}}\|_2.$$

It follows that with probability at least $1 - \delta$,

$$\begin{aligned} &\|(\mathbf{I}_M - \mathbf{U}_K \mathbf{U}_K^H) \tilde{\mathbf{U}}\|_2 = \|(\mathbf{I}_M - \tilde{\mathbf{U}} \tilde{\mathbf{U}}^H) \mathbf{U}_K\|_2 \\ &\leq [1 + o(1)] \frac{\sqrt{MK}}{\delta} \left(\frac{\sigma_{K+1}(\mathbf{S})}{\sigma_K(\mathbf{S})}\right)^{t+1}. \end{aligned} \quad (37)$$

We have that

$$\begin{aligned} &\|(\mathbf{I}_M - \mathbf{U}_K \mathbf{U}_K^H) \mathbf{a}\|_2 \\ &\leq \|(\mathbf{I}_M - \mathbf{U}_K \mathbf{U}_K^H) \tilde{\mathbf{U}} \tilde{\mathbf{U}}^H \mathbf{a}\|_2 \\ &\quad + \|(\mathbf{I}_M - \mathbf{U}_K \mathbf{U}_K^H) (\mathbf{I}_M - \tilde{\mathbf{U}} \tilde{\mathbf{U}}^H) \mathbf{a}\|_2 \\ &\leq \|(\mathbf{I}_M - \mathbf{U}_K \mathbf{U}_K^H) \tilde{\mathbf{U}} \tilde{\mathbf{U}}^H \mathbf{a}\|_2 + \|(\mathbf{I}_M - \tilde{\mathbf{U}} \tilde{\mathbf{U}}^H) \mathbf{a}\|_2. \end{aligned} \quad (38)$$

It follows from (37) and (38) that

$$\begin{aligned} &\|(\mathbf{I}_M - \mathbf{U}_K \mathbf{U}_K^H) \mathbf{a}\|_2 - \|(\mathbf{I}_M - \tilde{\mathbf{U}} \tilde{\mathbf{U}}^H) \mathbf{a}\|_2 \\ &\leq \|(\mathbf{I}_M - \mathbf{U}_K \mathbf{U}_K^H) \tilde{\mathbf{U}}\|_2 \|\mathbf{a}\|_2 \\ &\leq [1 + o(1)] \frac{\sqrt{MK}}{\delta} \left(\frac{\sigma_{K+1}(\mathbf{S})}{\sigma_K(\mathbf{S})}\right)^{t+1} \|\mathbf{a}\|_2, \end{aligned}$$

where the latter inequality holds with probability at least $1 - \delta$. Equivalently,

$$\begin{aligned} &\|(\mathbf{I}_M - \tilde{\mathbf{U}} \tilde{\mathbf{U}}^H) \mathbf{a}\|_2 - \|(\mathbf{I}_M - \mathbf{U}_K \mathbf{U}_K^H) \mathbf{a}\|_2 \\ &\geq -[1 + o(1)] \frac{\sqrt{MK}}{\delta} \left(\frac{\sigma_{K+1}(\mathbf{S})}{\sigma_K(\mathbf{S})}\right)^{t+1} \|\mathbf{a}\|_2, \end{aligned}$$

Thus, with probability at least $1 - \delta$,

$$\begin{aligned} \sqrt{\frac{P_{\text{music}}}{\tilde{P}_{\text{music}}}} &= \frac{\|(\mathbf{I} - \tilde{\mathbf{U}} \tilde{\mathbf{U}}^H) \mathbf{a}\|_2}{\|(\mathbf{I} - \mathbf{U}_K \mathbf{U}_K^H) \mathbf{a}\|_2} \\ &\geq 1 - [1 + o(1)] \frac{\sqrt{MK}}{\delta} \left(\frac{\sigma_{K+1}(\mathbf{S})}{\sigma_K(\mathbf{S})}\right)^{t+1} \frac{\|\mathbf{a}\|_2}{\|(\mathbf{I} - \mathbf{U}_K \mathbf{U}_K^H) \mathbf{a}\|_2}. \end{aligned}$$

By further applying the inequality in eq. (32), we have

$$\frac{\|\mathbf{a}\|_2}{\|(\mathbf{I} - \mathbf{U}_K \mathbf{U}_K^H) \mathbf{a}\|_2} \leq \sqrt{M}.$$

by which the theorem can be proved, i.e.

$$\sqrt{\frac{P_{\text{music}}}{P_{\text{music}}}} = \frac{\|(\mathbf{I} - \mathbf{U}_K \mathbf{U}_K^H) \mathbf{a}\|_2}{\|(\mathbf{I} - \mathbf{U}_K \mathbf{U}_K^H) \mathbf{a}\|_2} \geq 1 - \frac{\sqrt{M^2 K}}{\delta} \left(\frac{\sigma_{K+1}(\mathbf{S})}{\sigma_K(\mathbf{S})} \right)^{t+1}.$$

□

REFERENCES

- [1] W. D. Jones, "Keeping cars from crashing," *IEEE Spectrum*, vol. 38, no. 9, pp. 40–45, 2001.
- [2] D. Guizzo, "How google's self-driving car works," *IEEE Spectrum Online*, vol. 18, 2011.
- [3] E. P. Blasch, A. Lakhota, and G. Seetharaman, "Unmanned vehicles come of age: The darpa grand challenge," *Computer*, vol. 39, no. 12, pp. 26–29, 2006.
- [4] K. Alonzo, A. Stentz, O. Amidi, M. Bode, D. Bradley, A. Diazcalderon, M. Happold, H. Herman, R. Mandelbaum, and T. Pilarski, "Toward reliable off road autonomous vehicles operating in challenging environments," in *Proc of International Symposium on Experimental Robotics*, 2004.
- [5] M. Murad, I. Bilik, M. Friesen, J. Nickolaou, J. Salinger, K. Geary, and J. S. Colburn, "Requirements for next generation automotive radars," pp. 1–6, 2013.
- [6] C. Waldschmidt and H. H. Meinel, "Future trends and directions in radar concerning the application for autonomous driving," pp. 1719–1722, 2014.
- [7] J. Hasch, E. Topak, R. Schnabel, T. Zwick, R. Weigel, and C. Waldschmidt, "Millimeter-wave technology for automotive radar sensors in the 77 ghz frequency band," *IEEE Transactions on Microwave Theory and Techniques*, vol. 60, no. 3, pp. 845–860, 2012.
- [8] A. Natarajan, A. Komijani, X. Guan, A. Babakhani, and A. Hajimiri, "A 77-ghz phased-array transceiver with on-chip antennas in silicon: Transmitter and local lo-path phase shifting," *IEEE Journal of Solid-state Circuits*, vol. 41, no. 12, pp. 2807–2819, 2006.
- [9] I. Gresham, N. Jain, T. Budka, A. Alexanian, N. Kinayman, B. Ziegner, S. Brown, and P. Staecker, "A compact manufacturable 76-77-ghz radar module for commercial acc applications," *IEEE Transactions on Microwave Theory and Techniques*, vol. 49, no. 1, pp. 44–58, 2001.
- [10] W. Mayer, A. Gronau, W. Menzel, and H. Leier, "A compact 24 ghz sensor for beam-forming and imaging," pp. 1–6, 2006.
- [11] J. Li and P. Stoica, "Mimo radar with colocated antennas," *IEEE Signal Processing Magazine*, vol. 24, no. 5, pp. 106–114, 2007.
- [12] I. Bilik, S. Villeval, D. Brodeski, H. Ringel, O. Longman, P. Goswami, C. Y. B. Kumar, S. Rao, P. Swami, A. Jain, *et al.*, "Automotive multi-mode cascaded radar data processing embedded system," in *Proceedings of 2018 IEEE Radar Conference*, pp. 1–6, 2018.
- [13] F. Gini, A. D. Maio, and L. Patton, "Waveform design and diversity for advanced radar systems," p. 552, 2012.
- [14] S. Patole, M. Torlak, D. Wang, and M. Ali, "Automotive radars: A review of signal processing techniques," *IEEE Signal Processing Magazine*, vol. 34, no. 2, pp. 22–35, 2017.
- [15] A. G. Stove, "Linear fmcw radar techniques," *Proceedings of the IEEE*, 1992.
- [16] C. H. Lin, Y. S. Wu, Y. L. Yeh, S. H. Weng, G. Y. Chen, C. H. Shen, and H. Y. Chang, "A 24-ghz highly integrated transceiver in 0.5- μm e/dp-het process for fmcw automotive radar applications," in *Microwave Conference Proceedings*, pp. 512–515, 2011.
- [17] G. Babur, O. A. Krasnov, A. Yarovsky, and P. Aubry, "Nearly orthogonal waveforms for mimo fmcw radar," *IEEE Transactions on Aerospace & Electronic Systems*, vol. 49, no. 3, pp. 1426–1437, 2013.
- [18] P. Kumari, J. Choi, N. Gonzalezprelcic, and R. W. Heath, "Ieee 802.11ad-based radar: An approach to joint vehicular communication-radar system," *IEEE Transactions on Vehicular Technology*, vol. 67, no. 4, pp. 3012–3027, 2018.
- [19] D. Kok and J. S. Fu, "Signal processing for automotive radar," in *Radar Conference, 2005 IEEE International*, pp. 842–846, 2005.
- [20] J. Wenger, "Automotive radar - status and perspectives," in *Compound Semiconductor Integrated Circuit Symposium, 2005 (CSIC '05)*, p. 4 pp., 2005.
- [21] R. O. Schmidt, "Multiple emitter location and signal parameter estimation," *IEEE Transactions on Antennas and Propagation*, vol. 34, no. 3, pp. 276–280, 1986.
- [22] R. H. Roy and T. Kailath, "Esprit-estimation of signal parameters via rotational invariance techniques," *IEEE Transactions on Acoustics, Speech, and Signal Processing*, vol. 37, no. 7, pp. 984–995, 1989.
- [23] H. Krim and M. Viberg, "Two decades of array signal processing research: the parametric approach," *IEEE Signal Processing Magazine*, vol. 13, no. 4, pp. 67–94, 1996.
- [24] M. D. Zoltowski, G. M. Kautz, and S. D. Silverstein, "Beamspace root-music," *IEEE Transactions on Signal Processing*, vol. 41, no. 1, pp. 344–364, 1993.
- [25] H. D. Simon, "The lanczos algorithm with partial reorthogonalization," *Mathematics of Computation*, vol. 42, no. 165, pp. 115–142, 1984.
- [26] S. Marcos, A. Marsal, and M. Benidir, "The propagator method for source bearing estimation," *Signal Processing*, vol. 42, no. 2, pp. 121–138, 1995.
- [27] S. Marcos, A. Marsal, and M. Benidir, "Performances analysis of the propagator method for source bearing estimation," in *Acoustics, Speech, & Signal Processing, on IEEE International Conference*, 1994.
- [28] N. Tayem and H. M. Kwon, "L-shape 2-dimensional arrival angle estimation with propagator method," *IEEE Trans Antennas & Propagat*, vol. 1, no. 5, pp. 1622–1630, 2005.
- [29] J. Benesty, J. Chen, and Y. Huang, "A generalized mvdr spectrum," *IEEE Signal Processing Letters*, vol. 12, no. 12, pp. 827–830, 2005.
- [30] D. Oh and J. Lee, "Low-complexity range-azimuth fmcw radar sensor using joint angle and delay estimation without svd and evd," *IEEE Sensors Journal*, vol. 15, no. 9, pp. 4799–4811, 2015.
- [31] F. Engels, P. Heidenreich, A. M. Zoubir, F. K. Jondral, and M. Wintermantel, "Advances in automotive radar: A framework on computationally efficient high-resolution frequency estimation," *IEEE Signal Processing Magazine*, vol. 34, no. 2, pp. 36–46, 2017.
- [32] M. Y. Keegan Garcia and A. Purkovic, "Robust traffic and intersection monitoring using millimeter wave sensors," tech. rep., Texas Instruments Incorporated (TI), May 2018.
- [33] K. Ramasubramanian, "Using a complex-baseband architecture in FMCW radar systems," tech. rep., Texas Instruments Incorporated (TI), May 2017.
- [34] H. L. V. Trees, *Optimum Array Processing: Detection, Estimation, and Modulation Theory*. New York: John Wiley & Sons, Inc., 2001.
- [35] R. O. Schmidt, "A signal subspace approach to multiple emitter location spectral estimation," *Ph.d.thesis Stanford University*, 1981.
- [36] P. Stoica and N. Arye, "Music, maximum likelihood, and cramer-rao bound," *IEEE Transactions on Acoustics, Speech, and Signal Processing*, vol. 37, no. 5, pp. 720–741, 1989.
- [37] S. Fortunati, L. Sanguinetti, M. Greco, and F. Gini, "Scaling up mimo radar for target detection," pp. 4165–4169, 2019.
- [38] P. Vallet, X. Mestre, and P. Loubaton, "Performance analysis of an improved music doa estimator," *IEEE Transactions on Signal Processing*, vol. 63, no. 23, pp. 6407–6422, 2015.
- [39] X. Mestre and M. A. Lagunas, "Modified subspace algorithms for doa estimation with large arrays," *IEEE Transactions on Signal Processing*, vol. 56, no. 2, pp. 598–614, 2008.
- [40] W. Liao and A. Fannjiang, "Music for single-snapshot spectral estimation: Stability and super-resolution," *Applied & Computational Harmonic Analysis*, vol. 40, no. 1, pp. 33–67, 2014.
- [41] J. W. Odendaal, E. Barnard, and C. W. I. Pistorius, "Two-dimensional superresolution radar imaging using the music algorithm," *IEEE Transactions on Antennas and Propagation*, vol. 42, no. 10, pp. 1386–1391, 1994.
- [42] F. Belfiori, W. V. Rossum, and P. Hoogeboom, "Application of 2d music algorithm to range-azimuth fmcw radar data," in *Proc. of Radar Conference*, pp. 242–245, 2013.
- [43] S. Wang, A. Gittens, and M. W. Mahoney, "Scalable kernel k-means clustering with Nystrom approximation: Relative-error bounds," *Journal of Machine Learning Research*, vol. 20, no. 12, pp. 1–49, 2019.
- [44] P. Drineas and M. W. Mahoney, "On the Nystrom method for approximating a gram matrix for improved kernel-based learning," *Journal of Machine Learning Research*, vol. 6, pp. 2153–2175, 2005.
- [45] D. P. Woodruff, "Sketching as a tool for numerical linear algebra," *Foundations and Trends® in Theoretical Computer Science*, vol. 10, no. 1–2, pp. 1–157, 2014.
- [46] J. A. Tropp, A. Yurtsever, M. Udell, and V. Cevher, "Fixed-rank approximation of a positive-semidefinite matrix from streaming data," in *Advances in Neural Information Processing Systems (NIPS)*, 2017.

- [47] A. Gittens and M. W. Mahoney, “Revisiting the Nystrom method for improved large-scale machine learning,” *Journal of Machine Learning Research*, vol. 17, no. 1, pp. 3977–4041, 2016.
- [48] S. Wang, L. Luo, and Z. Zhang, “SPSD matrix approximation via column selection: Theories, algorithms, and extensions,” *Journal of Machine Learning Research*, vol. 17, no. 49, pp. 1–49, 2016.
- [49] R. Vershynin, “Introduction to the non-asymptotic analysis of random matrices,” *arXiv preprint arXiv:1011.3027*, 2010.
- [50] M. Rudelson and R. Vershynin, “The Littlewood–Offord problem and invertibility of random matrices,” *Advances in Mathematics*, vol. 218, no. 2, pp. 600–633, 2008.
- [51] T. Tao and V. Vu, “Random matrices: The distribution of the smallest singular values,” *Geometric And Functional Analysis*, vol. 20, no. 1, pp. 260–297, 2010.
- [52] P. Arbenz, “Lecture notes on solving large scale eigenvalue problems,” *D-MATH, EHT Zurich*, vol. 2, 2012.